

1990

# Incorporation of a rectangular void into a three-dimensional neutron diffusion nodal model

Mohamed Boussoufi  
*Iowa State University*

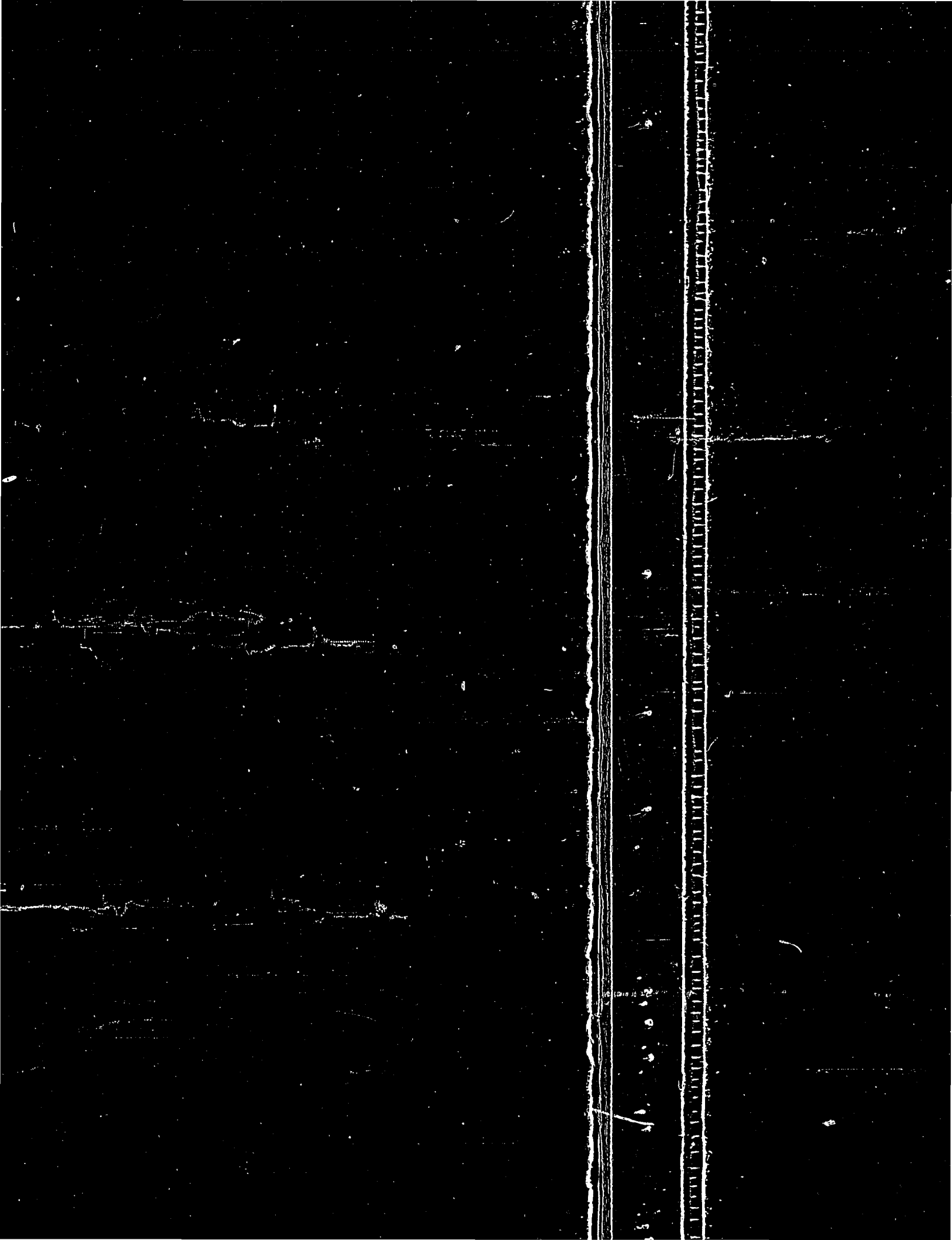
Follow this and additional works at: <https://lib.dr.iastate.edu/rtd>

 Part of the [Nuclear Engineering Commons](#)

## Recommended Citation

Boussoufi, Mohamed, "Incorporation of a rectangular void into a three-dimensional neutron diffusion nodal model" (1990).  
*Retrospective Theses and Dissertations*. 11246.  
<https://lib.dr.iastate.edu/rtd/11246>

This Dissertation is brought to you for free and open access by the Iowa State University Capstones, Theses and Dissertations at Iowa State University Digital Repository. It has been accepted for inclusion in Retrospective Theses and Dissertations by an authorized administrator of Iowa State University Digital Repository. For more information, please contact [digirep@iastate.edu](mailto:digirep@iastate.edu).



5

91

00420

U·M·I

MICROFILMED 1990

## **INFORMATION TO USERS**

The most advanced technology has been used to photograph and reproduce this manuscript from the microfilm master. UMI films the text directly from the original or copy submitted. Thus, some thesis and dissertation copies are in typewriter face, while others may be from any type of computer printer.

**The quality of this reproduction is dependent upon the quality of the copy submitted.** Broken or indistinct print, colored or poor quality illustrations and photographs, print bleedthrough, substandard margins, and improper alignment can adversely affect reproduction.

In the unlikely event that the author did not send UMI a complete manuscript and there are missing pages, these will be noted. Also, if unauthorized copyright material had to be removed, a note will indicate the deletion.

Oversize materials (e.g., maps, drawings, charts) are reproduced by sectioning the original, beginning at the upper left-hand corner and continuing from left to right in equal sections with small overlaps. Each original is also photographed in one exposure and is included in reduced form at the back of the book.

Photographs included in the original manuscript have been reproduced xerographically in this copy. Higher quality 6" x 9" black and white photographic prints are available for any photographs or illustrations appearing in this copy for an additional charge. Contact UMI directly to order.

# **U·M·I**

University Microfilms International  
A Bell & Howell Information Company  
300 North Zeeb Road, Ann Arbor, MI 48106-1346 USA  
313/761-4700 800/521-0600



**Order Number 9100420**

**Incorporation of a rectangular void into a three-dimensional  
neutron diffusion nodal model**

**Boussoufi, Mohamed, Ph.D.**

**Iowa State University, 1990**

**U·M·I**  
300 N. Zeeb Rd.  
Ann Arbor, MI 48106



**Incorporation of a rectangular void into  
a three-dimensional neutron diffusion  
nodal model**

by

Mohamed Boussoufi

A Dissertation Submitted to the  
Graduate Faculty in Partial Fulfillment of the  
Requirements for the Degree of  
DOCTOR OF PHILOSOPHY

Major: Nuclear Engineering

Approved:

Signature was redacted for privacy.

In Charge of Major Work

Signature was redacted for privacy.

For the Major Department

Signature was redacted for privacy.

For the Graduate College

Iowa State University  
Ames, Iowa  
1990

Copyright © Mohamed Boussoufi, 1990. All rights reserved.

## TABLE OF CONTENTS

<b>1.</b>	<b>INTRODUCTION</b> . . . . .	1
<b>2.</b>	<b>LITERATURE REVIEW</b> . . . . .	3
<b>3.</b>	<b>THE RECTANGULAR VOID</b> . . . . .	8
3.1	Void Configuration and Coordinates System . . . . .	8
3.2	The Source Face . . . . .	10
<b>4.</b>	<b>THEORY</b> . . . . .	14
4.1	Problem Statement . . . . .	14
4.2	Mathematical Formulation . . . . .	14
<b>5.</b>	<b>FLOW RATE EXPRESSIONS</b> . . . . .	18
5.1	The Bottom Face . . . . .	18
5.1.1	The isotropic flow rate . . . . .	21
5.1.2	The cosinazimuthal flow rate . . . . .	22
5.1.3	The sinazimuthal flow rate . . . . .	23
5.1.4	The radial flow rate . . . . .	23
5.2	The West Face . . . . .	24
5.2.1	The isotropic flow rate . . . . .	24
5.2.2	The cosinazimuthal flow rate . . . . .	25

5.2.3	The sinazimuthal flow rate . . . . .	25
5.2.4	The radial flow rate . . . . .	25
5.3	The East Face . . . . .	26
5.3.1	The isotropic flow rate . . . . .	26
5.3.2	The cosinazimuthal flow rate . . . . .	26
5.3.3	The sinazimuthal flow rate . . . . .	27
5.3.4	The radial flow rate . . . . .	27
5.4	The Top Face . . . . .	27
5.4.1	The isotropic flow rate . . . . .	27
5.4.2	The cosinazimuthal flow rate . . . . .	28
5.4.3	The sinazimuthal flow rate . . . . .	28
5.4.4	The radial flow rate . . . . .	28
5.5	The North Face . . . . .	29
5.5.1	The isotropic flow rate . . . . .	29
5.5.2	The cosinazimuthal flow rate . . . . .	30
5.5.3	The sinazimuthal flow rate . . . . .	30
5.5.4	The radial flow rate . . . . .	30
<b>6.</b>	<b>NEUTRON BALANCE(A BENCHMARK PROBLEM)</b> . . . . .	<b>32</b>
6.1	The Numerical Quadrature . . . . .	32
6.2	Neutron Balance . . . . .	34
6.2.1	The incoming flow rate . . . . .	35
6.2.2	The outcoming flow rate . . . . .	37
<b>7.</b>	<b>GENERAL EQUATIONS(CONCEPT OF TRANSFER MATRIX)</b> . . . . .	<b>38</b>

7.1	The Transfer Matrix . . . . .	38
7.1.1	Definition of the transfer matrix . . . . .	39
7.1.2	Construction of the transfer matrix . . . . .	40
7.2	Use of the Transfer Matrix in the Nodal Model . . . . .	41
7.3	Benchmark Problem . . . . .	41
7.3.1	The incoming flow rate (IFW) . . . . .	43
7.3.2	The outcoming flow rate (OFW) . . . . .	44
8.	<b>THE OVERALL TRANSFER MATRIX . . . . .</b>	<b>48</b>
9.	<b>MODEL LIMITATIONS . . . . .</b>	<b>53</b>
10.	<b>SUMMARY AND CONCLUSIONS . . . . .</b>	<b>56</b>
10.1	Summary . . . . .	56
10.2	Special Comments . . . . .	57
10.3	Conclusions . . . . .	59
11.	<b>SUGGESTIONS FOR FURTHER WORK . . . . .</b>	<b>60</b>
	<b>ACKNOWLEDGEMENTS . . . . .</b>	<b>64</b>
12.	<b>BIBLIOGRAPHY . . . . .</b>	<b>65</b>
13.	<b>APPENDIX A. DOUBLE INTEGRATION REDUCTION . . . . .</b>	<b>68</b>
13.1	Reduced Isotropic Functional $H_i(n, m, a, b, c)$ . . . . .	70
13.2	Reduced Azimuthal Functional $J_i(n, m, a, b, c)$ . . . . .	71
13.3	Reduced Azimuthal functional $K_i(n, m, a, b, c)$ . . . . .	71
13.4	Reduced Azimuthal Functional $L(n, m, a, b, c, d)$ . . . . .	72

14. APPENDIX B. FORTRAN PROGRAM FOR NUMERICAL INTEGRATION . . . . .	74
15. APPENDIX C. TEST FOR MODEL'S APPLICABILITY . . . .	81

## LIST OF TABLES

Table 6.1:	Flow rates components across the faces of the void for the sample problem . . . . .	37
Table 6.2:	Total Flow rates across the faces of the void for the sample problem . . . . .	37
Table 7.1:	Inbound neutron flow rates across faces of the void . . . . .	43
Table 7.2:	Flow rates components across faces of the void when the top face is the only source . . . . .	44
Table 7.3:	Total Flow rates across faces of the void when the top face is the only source . . . . .	44
Table 7.4:	Flow rates components across faces of the void when the bottom face is the only source . . . . .	45
Table 7.5:	Total Flow rates across faces of the void when the bottom face is the only source . . . . .	45
Table 7.6:	Flow rates components across faces of the void when the east face is the only source . . . . .	45
Table 7.7:	Total Flow rates across faces of the void when the east face is the only source . . . . .	45

Table 7.8:	Flow rates components across faces of the void when the west face is the only source . . . . .	46
Table 7.9:	Total Flow rates across faces of the void when the west face is the only source . . . . .	46
Table 7.10:	Flow rates components across faces of the void when the north face is the only source . . . . .	46
Table 7.11:	Total Flow rates across faces of the void when the north face is the only source . . . . .	46
Table 7.12:	Flow rates components across faces of the void when the south face is the only source . . . . .	47
Table 7.13:	Total Flow rates across faces of the void when the south face is the only source . . . . .	47
Table 7.14:	Total Flow rates across faces of the void (all faces being sources)	47
Table 9.1:	“Flat” void limiting dimension ( $\eta = \nu = 10.0$ ) . . . . .	55
Table 9.2:	“Long” void limiting dimension ( $\nu = 10.0$ ) . . . . .	55

## LIST OF FIGURES

Figure 2.1:	The spherical coordinate system . . . . .	4
Figure 3.1:	Three dimensional void and coordinates system . . . . .	9
Figure 3.2:	Possible void locations where not all faces are sources . . . . .	11
Figure 3.3:	The adjacent node . . . . .	12
Figure 3.4:	Angles $\theta$ and $\psi$ . . . . .	13
Figure 4.1:	Exit window configuration . . . . .	15
Figure 4.2:	Angle $\alpha$ . . . . .	16
Figure 5.1:	The bottom face variables . . . . .	19
Figure 8.1:	A void and its adjacent node . . . . .	48
Figure 9.1:	A Flat void . . . . .	54
Figure 9.2:	A Long void . . . . .	54
Figure 11.1:	An accumulation of three voids . . . . .	62

## 1. INTRODUCTION

The application of the neutron transport equation to the treatment of voids in a nuclear reactor is somewhat a puzzling task. Since the cross sections involved have very low values, practically zero for a gas, their insertion into the steady state transport equation with no source term, as suggested by the void composition, would lead to a trivial equation. Schemes using the finite element method [1], have lead to the complexity of breaking the transport equation into 2 equations of even and odd parity. The approach developed in the present work aims to avoid the burden of such an undertaking.

Although voids in a nuclear reactor may assume different shapes (e.g., spherical in a gas cooled reactor), only a rectangular geometry will be treated here. It is assumed that other shapes are to be the topic of further work.

The motivation for the treatment of the streaming of neutrons inside a cavity has been derived from the need to account for voids that occupy nodal positions in the nodal method [2]. The nodal method is a scheme used to approximate the transport solution [3]. This method suggested, by Graves [4], consists of subdividing the reactor into an array of nodal volumes, usually equal volumes; each nodal volume is then represented by a set of space-and-energy averaged neutronic parameters that describe its neutron multiplication and transport properties.

An immediate application of the present study would be in shielding analysis, to account for neutron transport within a rectangular duct.

A word of caution should be mentioned here however. Shielding problems require that one use a high order approximation to the angular fluxes for a correct design of the shielding components; and, since the present study concerns itself only with the P1 approximation, the results would not be directly applicable. Hence, the shielding analyst should keep in mind that this method provides only a beginning estimate of the neutron streaming. A more adequate method would require higher components in the angular fluxes ( $P_N$  equations), a method which would be a logical extension of this research work.

## 2. LITERATURE REVIEW

The working frame of this analysis is the P1 approximation to the angular flux which assumes a weak dependence on angle<sup>1</sup>. After expanding the angular flux in angle and neglecting the terms of higher than linear order [5], we may write:

$$\varphi(r, \hat{\Omega}) \simeq \frac{\phi}{4\pi} + \frac{3}{4\pi}(J_x \Omega_x + J_y \Omega_y + J_z \Omega_z) \quad (2.1)$$

where:

$\hat{\Omega}$ =angular direction

$\varphi(r, \hat{\Omega})$ = steady state angular flux

$\phi$ = angle-integrated flux

$J_x, J_y, J_z$ = components of the neutron current  $J$

$\Omega_x, \Omega_y, \Omega_z$ =components of  $\hat{\Omega}$

Fick's law<sup>2</sup> relates  $J$  and  $\phi$  through:

$$J(r) = -D\nabla\phi(r) \quad (2.2)$$

where  $D$  is the diffusion coefficient.

In the spherical coordinate system  $(r, \theta, \psi)$  (see Figure 2.1):

---

<sup>1</sup> Assumption violated near boundaries, near localized sources and in strongly absorbing media.

<sup>2</sup> Valid only in the diffusion approximation.

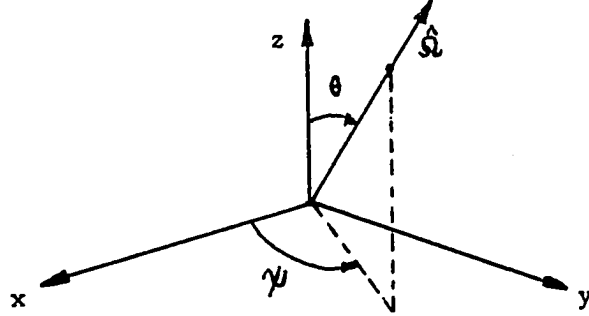


Figure 2.1: The spherical coordinate system

$$\Omega_x = \sin \theta \cos \psi \quad (2.3)$$

$$\Omega_y = \sin \theta \sin \psi \quad (2.4)$$

$$\Omega_z = \cos \theta \quad (2.5)$$

Inserting Eqs. (2.2), (2.3), (2.4) and (2.5) into (2.1) we reach:

$$\varphi(r, \hat{\Omega}) \simeq \frac{\phi}{4\pi} - \frac{3D}{4\pi} \left( \frac{\partial \phi}{\partial x} \sin \theta \cos \psi + \frac{\partial \phi}{\partial y} \sin \theta \sin \psi + \frac{\partial \phi}{\partial z} \cos \theta \right) \quad (2.6)$$

which can be written in more usable form:

$$\varphi(r, \hat{\Omega}) \simeq \phi_0(x, y, z) + \phi_1(x, y, z) \sin \theta \cos \psi + \phi_2(x, y, z) \sin \theta \sin \psi + \phi_3(x, y, z) \cos \theta \quad (2.7)$$

where:

$$\begin{aligned} \phi_0(x, y, z) &= \frac{\phi}{4\pi} \\ \phi_1(x, y, z) &= -\frac{3D}{4\pi} \frac{\partial \phi}{\partial x} \\ \phi_2(x, y, z) &= -\frac{3D}{4\pi} \frac{\partial \phi}{\partial y} \\ \phi_3(x, y, z) &= -\frac{3D}{4\pi} \frac{\partial \phi}{\partial z} \end{aligned} \quad (2.8)$$

This form of the angular flux will be used throughout the remainder of the present analysis.

The approach adopted in this analysis uses the “radiation like” nature of neutrons. Faces of the void are regarded as sources of neutrons with a source strength density equal to  $\varphi(r, \Omega)\Omega.dS$ , where  $dS$  is the unit surface area with unit normal. For a geometrically plane face the source strength density reduces to  $\varphi(r, \Omega) \cos \theta$ , where  $\theta$  is the angle relative to the normal to the face. The response  $R$  of a neutron detector placed inside the void would then be:

$$R = \int_s \varphi(r, \Omega) \cos \theta d\Omega \quad (2.9)$$

where the integration is over the source faces and  $d\Omega$  is the solid angle with which an element of source is seen by the point detector:

$$d\Omega = \frac{dS \cos \theta}{r^2}$$

This concept of detector response is a very common practice in many radiation shielding problems [6]. Radiation from uniform rectangular sources was investigated by Hubbel et al. [6]. They evaluated the integral (2.9) numerically using a polar form of the integrand. In the present analysis a cartesian form is used because of the nature of the problem. Hubbel, Bach and Lamkin [6] were primarily interested in finding the gamma radiation dose rate at any point within a rectangular underground shelter whose ceiling is the active source of radiations. They have found for this problem, a polar form to be appropriate.

Maerker et al. in [7] used Hubbel’s findings [6] to deal with neutron attenuation in rectangular ducts where they say:

“ Neutron streaming through rectangular ducts is important to reactor plant design and to shelter design against radiation from nuclear weapons bursts. The research effort has generally been directed toward the shelter problem, and the significant results are for large concrete-walled ducts. These results have some applicability to reactor plants for large ventilating ducts, labyrinthine access ways, and pipe chases.”

Although their work bears some similarity with the present one, their goals are different.

Ackroyd et al. [1] dealt with the treatment of voids using finite element transport methods. His results are applicable only to the two-dimensional case and involve the so-called even parity neutron transport equation. He prescribes two methods to solve the problem: The first one is called the “ Method of extrapolation” which is based on the idea of a best approximation in a vector space from functional analysis, these results have not been published. The second method for obtaining solutions in the void is based on the idea of absorbing neutrons in a “void” with a cross section  $\sigma_1$  and then releasing these neutrons (along their original direction) within the “void”, which now has a lower absorption cross section  $\sigma_2$ . The iterative procedure continues until the absorption sources within the “void” almost disappear. The solutions obtained using the iterative scheme give lower bounds to the exact solution in the void,  $\phi_0^+(r, \Omega)$ .

$$\phi_I^+(r, \Omega) \leq \phi_0^+(r, \Omega)$$

These results also have not been published.

Early work in void-related problems was done by Behrens [8]. He focused mainly on how the migration length of neutrons in a reactor is affected by the presence of holes in a reactor. Thus he dealt with a collection of voids and his results are not directly relevant for this analysis. Benoist [9] formulated and computed the diffusion

coefficient for a nuclear system containing cavities.

Random voids in neutron shields were investigated by Burrus in [7]. His research efforts, were directed towards the transmission of neutron radiation. He writes:

“ As is true for gamma rays, the accidental alignment of low attenuating voids increases the transmission over that which would be expected if the shields were homogenized (i.e., finely pulverized and blended uniformly without changing the volume or weight).”

Research work as reviewed in the literature is not directly applicable for use in the treatment of voids within the nodal method. Therefore this research is relevant for developing a model for inclusion in the nodal method.

### 3. THE RECTANGULAR VOID

#### 3.1 Void Configuration and Coordinates System

The void used in this study has a three-dimensional configuration, its shape is a parallelepiped. The chosen coordinate system has an orientation such that its z axis is perpendicular to the ABCD face and its center O is located at the center of the void (see Figure 3.1). The following data will be used for the void:

(1) Void dimensions and volume:

$$AB = 2\nu$$

$$AD = 2\eta$$

$$AE = 2\mu$$

$$\text{Void volume} = 8\eta\nu\mu$$

(2) Coordinates of points A,B,C,D,E,F,G,H: (see Figure 3.1)

$$A(\eta, \nu, -\mu) \quad E(\eta, \nu, \mu)$$

$$B(\eta, -\nu, -\mu) \quad F(\eta, -\nu, \mu)$$

$$C(-\eta, -\nu, -\mu) \quad G(-\eta, -\nu, \mu)$$

$$D(-\eta, \nu, -\mu) \quad H(-\eta, \nu, \mu)$$

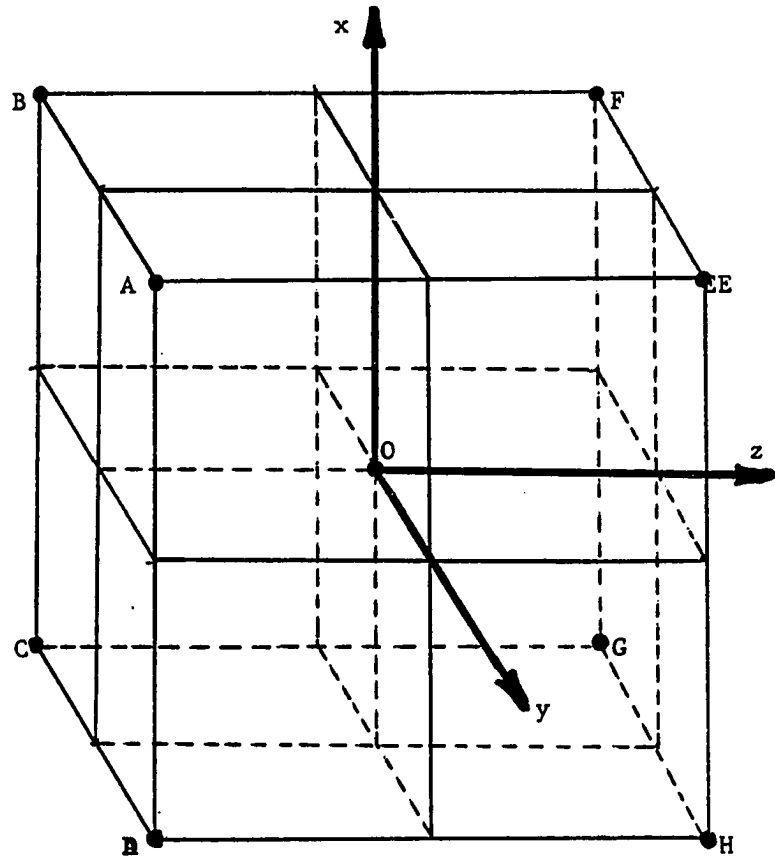


Figure 3.1: Three dimensional void and coordinates system

The following nomenclature will be adopted for the 6 faces of the void:

face ABCD: south face (source face)

face EFGH: north face

face BCGF: west face

face ADHE: east face

face ABFE: top face

face CDHG: bottom face

### 3.2 The Source Face

As an introductory step to the “void equations” development, we will assume that only the south face is a source face; this means that neutrons streaming into the void will be only the ones entering through face ABCD incoming from a multiplying media located in a node adjacent to the south face. Since voids are usually surrounded by an active media, neutrons will be entering through all 6 faces (Nodal Method). It is however the intent of this work to generalize the result of the “one source face” step to account for the above situation where all 6 faces are sources. It must be said that depending on the void location all six faces may not be sources. These situations are depicted in Figure 3.2.

Within the P1 approximation, the angular flux  $\varphi$ , in a node adjacent to the void (see Figure 3.3), may be written as [5]:

$$\varphi(r, \Omega) = \phi_0(x, y, z) + \phi_1(x, y, z) \sin \theta \cos \psi + \phi_2(x, y, z) \sin \theta \sin \psi + \phi_3(x, y, z) \cos \theta \quad (3.1)$$

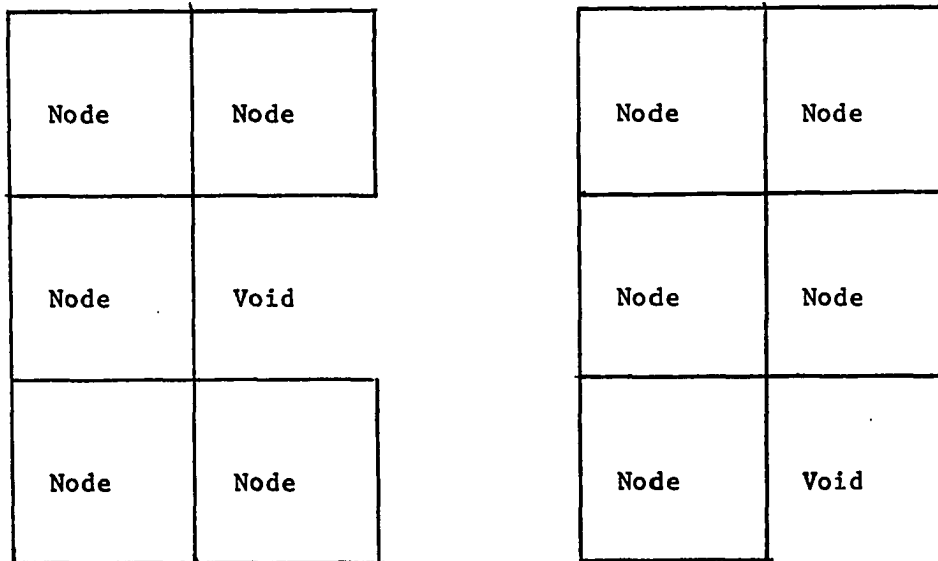


Figure 3.2: Possible void locations where not all faces are sources

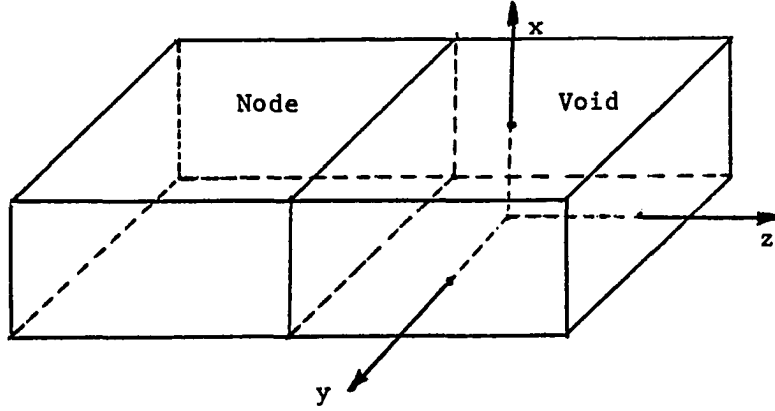


Figure 3.3: The adjacent node .

where the spatial fluxes are related by:

$$\phi_1(x, y, z) = -3D \frac{\partial \phi_0}{\partial x} \quad (3.2)$$

$$\phi_2(x, y, z) = -3D \frac{\partial \phi_0}{\partial y} \quad (3.3)$$

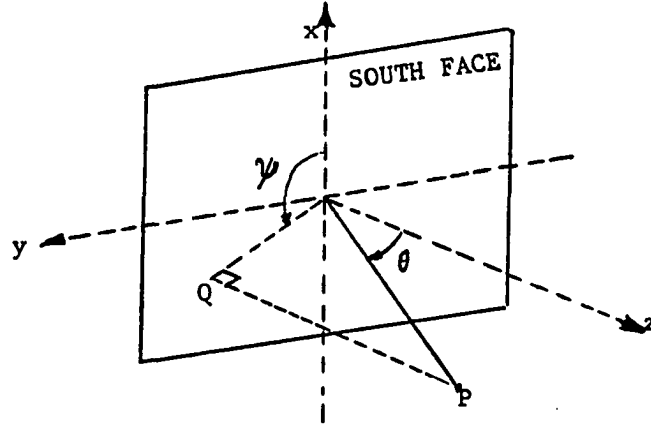
$$\phi_3(x, y, z) = -3D \frac{\partial \phi_0}{\partial z} \quad (3.4)$$

$D$  is the diffusion coefficient in the node adjacent to the void. Angles  $\theta$  and  $\psi$  are shown in Figure 3.4.

The angular flux  $\varphi_s$  for the south face can then be obtained by setting  $z = -\mu$  in Eq. (3.1). The angular flux  $\varphi_s$  which describe the spatial distribution of neutrons entering the void would then be given by:

$$\varphi_s(x, y, \theta, \psi) = \Phi_0(x, y) + \Phi_1(x, y) \sin \theta \cos \psi + \Phi_2(x, y) \sin \theta \sin \psi + \Phi_3(x, y) \cos \theta \quad (3.5)$$

In the diffusion nodal model [10], the nodal fluxes are determined as a power series of Legendre polynomials. In this work it is more convenient to use a straight power

Figure 3.4: Angles  $\theta$  and  $\psi$ 

series.

The spatial fluxes  $\Phi_0(x,y)$ ,  $\Phi_1(x,y)$ ,  $\Phi_2(x,y)$  and  $\Phi_3(x,y)$  can be expressed in terms of a polynomial expansion in  $x$  and  $y$  as:

$$\Phi_0(x,y) = \sum_n \sum_m a_{nm} x^n y^m \quad (3.6)$$

$$\Phi_1(x,y) = \sum_n \sum_m b_{nm} x^n y^m \quad (3.7)$$

$$\Phi_2(x,y) = \sum_n \sum_m c_{nm} x^n y^m \quad (3.8)$$

$$\Phi_3(x,y) = \sum_n \sum_m d_{nm} x^n y^m \quad (3.9)$$

A complete determination of  $\varphi_3$  is then subjected to an adequate choice of:

1. the polynomial degree ( $n$  and  $m$ )
2. the expansion coefficients  $a_{nm}$ ,  $b_{nm}$ ,  $c_{nm}$  and  $d_{nm}$ .

These latter can be readily determined from a transformation of the Legendre polynomials.

## 4. THEORY

### 4.1 Problem Statement

Upon entering the south face, the neutrons will exit from the node from all 5 surrounding faces, i.e., east, west, north, top and bottom. We are interested in finding the flow rate<sup>1</sup>(number of neutrons per second) that exit from a “window” located in any of the 5 surrounding faces. A “window”, as defined here, has a rectangular shape and is such that its sides are parallel to the sides of the face to which it belongs, see Figure 4.1. One can immediately see that the biggest possible size of a “window” is the whole face.

### 4.2 Mathematical Formulation

The flow rate of neutrons exiting from a “window” may be expressed as follows:

$$Flow\ rate = \int_s \int_w \varphi_s(x, y, \theta, \psi) \cos\theta d\Omega dS \quad (4.1)$$

the double surface integration is over the source face ( $s$ ) and the “window” ( $w$ ).  $\varphi_s(x, y, \theta, \psi) \cos\theta dS$  is the source strength of an increment of source face  $dS$  and  $d\Omega$  is the elementary solid angle which contains the neutrons traveling in direction  $\theta$  and

---

<sup>1</sup>If the average current is sought instead, divide flow rate by window’s area.

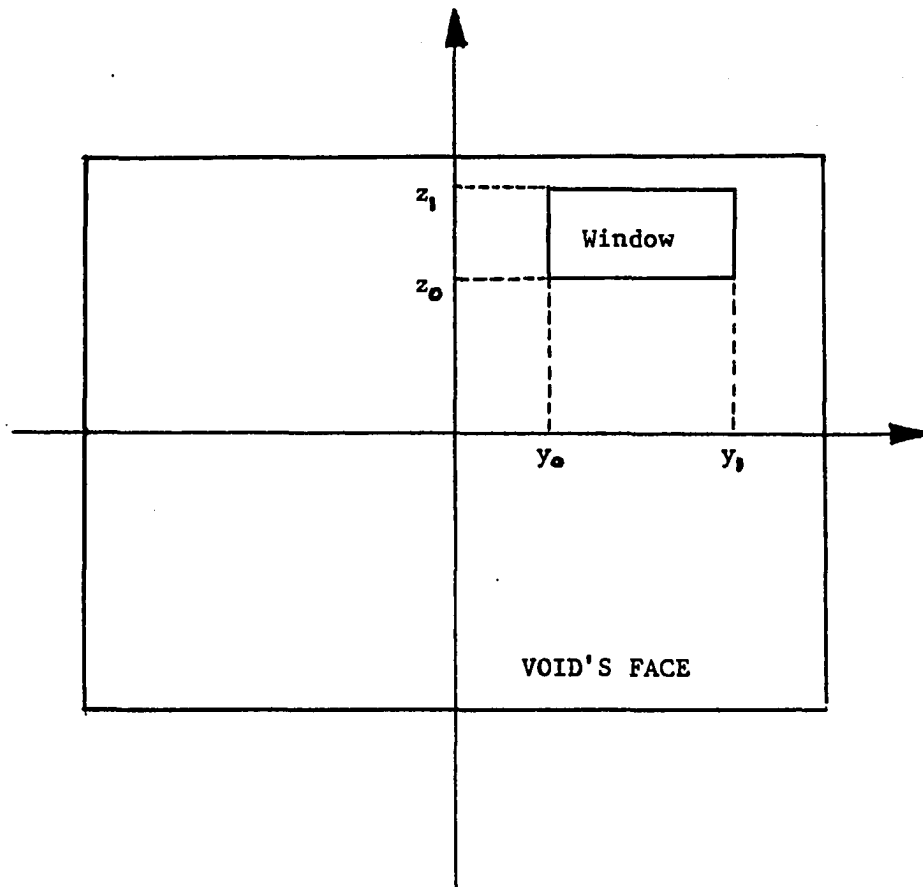
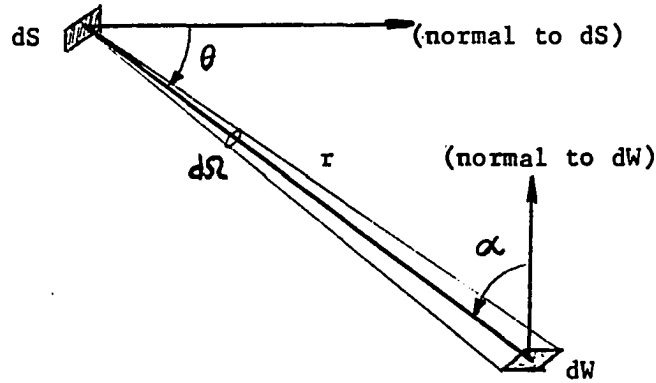


Figure 4.1: Exit window configuration

Figure 4.2: Angle  $\alpha$ 

incoming from  $dS$ :

$$d\Omega = \frac{\cos \alpha dW}{r^2} \quad (4.2)$$

where  $dW$  is a surface increment of the "window" (see Figure 4.2).

A complete expression for the flow rate is then:

$$\text{Flow rate} = \int_s \int_w \frac{\varphi_s(x, y, \theta, \psi) \cos \theta \cos \alpha dW dS}{r^2} \quad (4.3)$$

To handle the integration process, it is desirable to break the flow rate into four components (using the P1 approximation of the angular flux):

$$\text{Flow rate} = \text{Flow rate1} + \text{Flow rate2} + \text{Flow rate3} + \text{Flow rate4}$$

where:

$$\text{Flow rate1} = \int_s \int_w \frac{\Phi_0(x, y) \cos \theta \cos \alpha dW dS}{r^2} \quad (4.4)$$

which is the "isotropic" flow rate.

$$\text{Flow rate2} = \int_s \int_w \frac{\Phi_1(x, y) \cos \theta \sin \theta \cos \alpha \cos \psi dW dS}{r^2} \quad (4.5)$$

will be called the "cosinazimuthal" flow rate.

$$Flow\ rate3 = \int_s \int_w \frac{\Phi_2(x,y) \cos \theta \sin \theta \cos \alpha \sin \psi dW dS}{r^2} \quad (4.6)$$

will be called the "sinazimuthal" flow rate.

$$Flow\ rate4 = \int_s \int_w \frac{\Phi_3(x,y) \cos^2 \theta \cos \alpha dW dS}{r^2} \quad (4.7)$$

will be called the "radial" flow rate.

It is important to note that if a higher approximation to the angular flux ( $P_N$  equations) is used, additional components will appear in the expression of the neutron flow rate so that the integration process must include the contribution of these higher terms. These added contributions would be of importance, as discussed in the introduction, to the gamma ray shielding analyst.

## 5. FLOW RATE EXPRESSIONS

At this point the following notations need to be introduced. The flow rate across a particular "window" will be written using a "four letter" word. The first letter will stand for the window location, i.e, east, west, etc., the second for the flow rate component and the last two carry an abbreviation of the word "flow rate", i.e., FW.

examples:

NIFW: North isotropic flow rate

BRFW: Bottom radial flow rate

Hence, it can be seen that the first letter can only be N, W, E, B or T which stands for north, west, east, bottom and top respectively. The second letter can only be I, C, S or R which stands for isotropic, cosinazimuthal, sinazimuthal and radial respectively.

### 5.1 The Bottom Face

On Figure 5.1 are shown points M, H, P, N and K whose coordinates are needed to derive analytical expressions for  $\cos \theta$ ,  $\sin \theta$ ,  $\cos \psi$ ,  $\sin \psi$  and  $\cos \alpha$ .

These coordinates are:

$$M(x, y, -\mu) \quad N(-\eta, y', z')$$

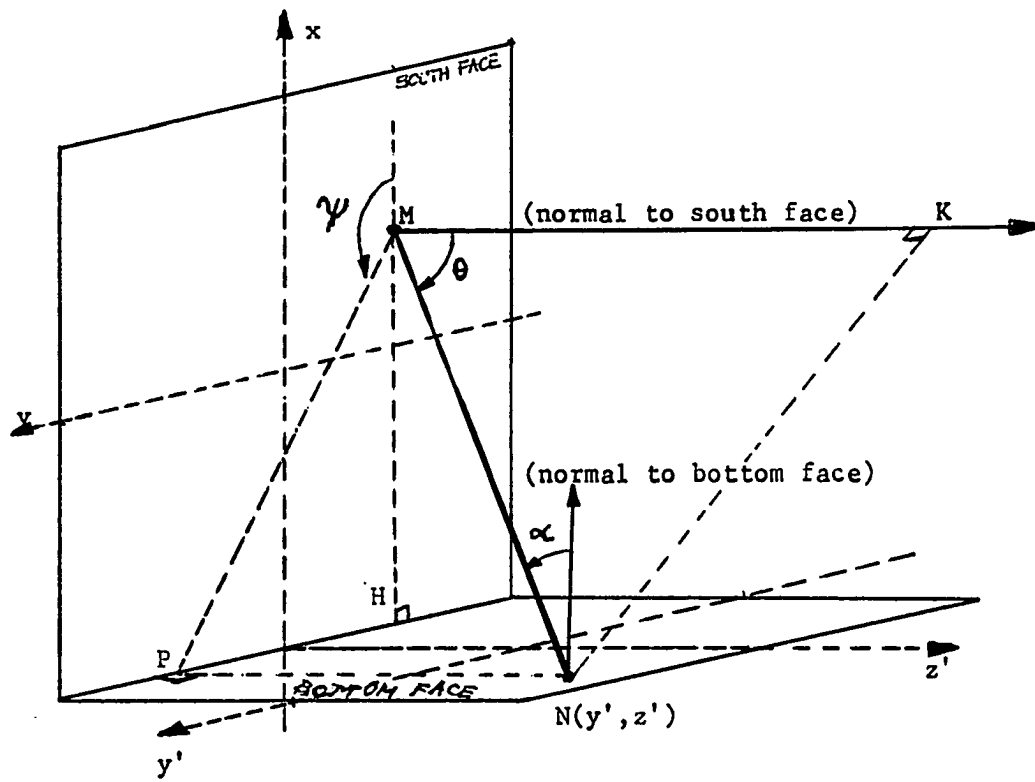


Figure 5.1: The bottom face variables

$$\begin{aligned}
& H(-\eta, y, -\mu) \quad P(-\eta, y', -\mu) \\
& \quad \quad \quad K(x, y, z')
\end{aligned}$$

Use of these coordinates leads to the following results:

$$\begin{aligned}
MH^2 &= (x + \eta)^2 \\
MP^2 &= (x + \eta)^2 + (y - y')^2 \\
HP^2 &= (y - y')^2 \\
MN^2 &= (x + \eta)^2 + (y - y')^2 + (z' + \mu)^2 \\
MK^2 &= (z' + \mu)^2 \\
NK &= MP
\end{aligned} \tag{5.1}$$

where MH, MP, HP, MN, MK, NK and MP are lengths of lines joining the corresponding points. Finally from these last relations one can infer that:

$$\begin{aligned}
\cos \theta &= \frac{(z' + \mu)}{MN} \\
\sin \theta &= \frac{\sqrt{(x + \eta)^2 + (y - y')^2}}{MN} \\
\cos \alpha &= \frac{(x + \eta)}{MN} \\
\cos \psi &= \frac{-(x + \eta)}{MP} \\
\sin \psi &= \frac{(y' - y)}{MP}
\end{aligned} \tag{5.2}$$

where:

$$MN = \sqrt{(x + \eta)^2 + (y - y')^2 + (z' + \mu)^2} \tag{5.3}$$

$$MP = \sqrt{(x + \eta)^2 + (y - y')^2} \tag{5.4}$$

### 5.1.1 The isotropic flow rate

According to Eq. (4.4) the isotropic flow rate for the bottom face is given by:

$$BIFW = \int_s \int_w \frac{\Phi_0(x, y) \cos \theta \cos \alpha dx dy dy' dz'}{r^2} \quad (5.5)$$

or

$$BIFW = \int_{-\eta}^{\eta} dx \int_{-\nu}^{\nu} S(x, y) dy \quad (5.6)$$

where  $S(x, y)$  is:

$$S(x, y) = \int_{y_0}^{y_1} \int_{z_0}^{z_1} \frac{\Phi_0(x, y) \cos \theta \cos \alpha dy' dz'}{r^2} \quad (5.7)$$

The parameters  $y_0, y_1, z_0$  and  $z_1$  are the "window" coordinates in the frame  $(y', z')$ , see Figure 4.1.

Using expressions of  $\cos \theta$  and  $\cos \alpha$  given by Eq. (5.2) one may write  $S(x, y)$  as:

$$S(x, y) = \Phi_0(x, y)(x + \eta) \int_{y_0}^{y_1} \int_{z_0}^{z_1} \frac{(z' + \mu) dy' dz'}{MN^4} \quad (5.8)$$

where  $r=MN$ .

The double integration over the window can easily be performed [11] to yield:

$$S(x, y) = \Phi_0(x, y)(x + \eta)(F_{01}(x, y) - F_{00}(x, y) + F_{10}(x, y) - F_{11}(x, y))$$

where:

$$F_{ij}(x, y) = \frac{1}{2\sqrt{(x + \eta)^2 + Z_i^2}} \arctan\left(\frac{y_j - y}{\sqrt{(x + \eta)^2 + Z_i^2}}\right) \quad (5.9)$$

with  $Z_i = z_i + \mu$ .

For the remaining double integration over the face, a numerical quadrature shall be used since an analytical solution has not been found to be possible. Although the

double integration can be reduced to a single integration (see APPENDIX A), the former has been preferred due to its simplicity in programming.

Making use of the polynomial formulation of  $\Phi_0(x, y)$  in Eq. (3.6) and normalizing the limits of integration one has the following result:

$$BIFW = \sum_n \nu \eta^{n+2} G_n \quad (5.10)$$

where:

$$G_n = \sum_n \nu^m a_{nm} (I_{nm}^{(01)} - I_{nm}^{(00)} + I_{nm}^{(10)} - I_{nm}^{(11)}) \quad (5.11)$$

The functional  $I_{nm}^{(ij)}$  is given by:

$$I_{nm}^{(ij)} = \int_{-1}^{+1} \int_{-1}^{+1} \frac{u^n v^m (u+1)}{2\sqrt{\eta^2(u+1)^2 + Z_i^2}} \arctan\left(\frac{y_j - \nu v}{\sqrt{\eta^2(u+1)^2 + Z_i^2}}\right) dudv \quad (5.12)$$

The functional  $I_{nm}^{(ij)}$  and all subsequent functionals will be computed through a suitable numerical quadrature.

### 5.1.2 The cosinazimuthal flow rate

Using Eq. (4.5) and Eq. (5.2) one can determine the cosinazimuthal flow rate as:

$$BCFW = - \int_s \int_w \frac{\Phi_1(x, y)(x + \eta)^2(z' + \mu) dW dS}{MN^5} \quad (5.13)$$

A similar integration process [11] to the one used for the isotropic case will yield the following end result:

$$BCFW = \sum_n \nu \eta^{n+3} G_n \quad (5.14)$$

where

$$G_n = \sum_m \nu^m b_{nm} (C_{nm}^{(11)} - C_{nm}^{(10)} + C_{nm}^{(00)} - C_{nm}^{(01)}) \quad (5.15)$$

The functional  $C_{nm}^{(ij)}$  is:

$$C_{nm}^{(ij)} = \int_{-1}^{+1} \int_{-1}^{+1} \frac{u^n (u+1)^2 v^m (y_j - \nu v) dudv}{3(\eta^2(u+1)^2 + Z_i^2) \sqrt{\eta^2(u+1)^2 + (y_j - \nu v)^2 + Z_i^2}} \quad (5.16)$$

### 5.1.3 The sinazimuthal flow rate

The sinazimuthal flow rate given through Eq. (4.6) is:

$$BSFW = \int_s \int_w \frac{\Phi_2(x, y)(x + \eta)(y' - y)(z' + \mu) dW dS}{MN^5} \quad (5.17)$$

Following the same procedure [11], one has:

$$BSFW = \sum_n \nu \eta^{n+2} G_n \quad (5.18)$$

where:

$$G_n = \sum_m \nu^m c_{nm} (S_{nm}^{(11)} - S_{nm}^{(10)} + S_{nm}^{(00)} - S_{nm}^{(01)}) \quad (5.19)$$

Functional  $S_{nm}^{(ij)}$  is given by:

$$S_{nm}^{(ij)} = \int_{-1}^{+1} \int_{-1}^{+1} \frac{u^n (u+1) v^m dudv}{3 \sqrt{\eta^2(u+1)^2 + Z_i^2 + (y_j - \nu v)^2}} \quad (5.20)$$

### 5.1.4 The radial flow rate

from Eq. (4.7) one has:

$$BRFW = \int_s \int_w \frac{\Phi_3(x, y)(x + \eta)(z' + \mu)^2 dW dS}{MN^5} \quad (5.21)$$

Carrying out the integration [11] will lead to:

$$BRFW = \sum_n \nu \eta^{n+2} G_n \quad (5.22)$$

where:

$$G_n = \sum_m \nu^m d_{nm} (R_{nm}^{(11)} - R_{nm}^{(10)} + R_{nm}^{(00)} - R_{nm}^{(01)}) \quad (5.23)$$

Functional  $R_{nm}^{(ij)}$  is:

$$R_{nm}^{(ij)} = \int_{-1}^{+1} \int_{-1}^{+1} \frac{u^n \nu^m}{3} \left( \frac{1}{\eta} \arctan\left(\frac{Z_i X_{ij}}{\eta(u+1)}\right) - \frac{(u+1)Z_i X_{ij}}{(\eta^2(u+1)^2 + Z_i^2)} \right) dudv \quad (5.24)$$

where:

$$X_{ij} = \sin\left(\arctan\left(\frac{y_j - \nu v}{\sqrt{\eta^2(u+1)^2 + Z_i^2}}\right)\right)$$

## 5.2 The West Face

The procedure used to derive the flow rate expressions for the west face (and for all subsequent faces) is very much similar to the one used for the bottom face, so the steps of the derivation will not be reproduced here, rather only results will be stated.

The steps used were basically:

- (1) Draw a picture of the angular configuration.
- (2) Obtain trigonometrical expressions for angles  $\theta$ ,  $\alpha$  and  $\psi$ .
- (3) Substitute the values of those angles into the flow rate expression and use the results of the bottom face with an appropriate switch of parameters. It turns out that if some parameters of integration are interchanged, e.g.,  $x$  with  $y$  and  $\eta$  with  $\nu$ , the integrals encountered are similar to the bottom face integrals.

### 5.2.1 The isotropic flow rate

After performing the appropriate transformations, one has:

$$WIFW = \sum_m \eta \nu^{m+2} G_m \quad (5.25)$$

$$G_m = \sum_n \eta^n a_{nm} (I_{nm}^{(01)} - I_{nm}^{(00)} + I_{nm}^{(10)} - I_{nm}^{(11)}) \quad (5.26)$$

$$I_{nm}^{(ij)} = \int_{-1}^{+1} \int_{-1}^{+1} \frac{u^n v^m (v+1)}{2\sqrt{\nu^2(v+1)^2 + Z_i^2}} \arctan\left(\frac{(x_j - \eta u)}{\sqrt{\nu^2(v+1)^2 + Z_i^2}}\right) dudv \quad (5.27)$$

### 5.2.2 The cosinazimuthal flow rate

$$WCFW = \sum_m \eta \nu^{m+2} G_m \quad (5.28)$$

$$G_m = \sum_n \eta^n b_{nm} (R_{nm}^{(11)} - R_{nm}^{(10)} + R_{nm}^{(00)} - R_{nm}^{(01)}) \quad (5.29)$$

$$R_{nm}^{(ij)} = \int_{-1}^{+1} \int_{-1}^{+1} \frac{u^n v^m (v+1) dudv}{3\sqrt{\nu^2(v+1)^2 + Z_i^2 + (x_j - \eta u)^2}} \quad (5.30)$$

### 5.2.3 The sinazimuthal flow rate

$$WSFW = \sum_m \eta \nu^{m+3} G_m \quad (5.31)$$

$$G_m = \sum_n \eta^n c_{nm} (S_{nm}^{(11)} - S_{nm}^{(10)} + S_{nm}^{(00)} - S_{nm}^{(01)}) \quad (5.32)$$

$$S_{nm}^{(ij)} = \int_{-1}^{+1} \int_{-1}^{+1} \frac{u^n v^m (v+1)^2 (x_j - \eta u) dudv}{3(\nu^2(v+1)^2 + Z_i^2)\sqrt{\nu^2(v+1)^2 + (x_j - \eta u)^2 + Z_i^2}} \quad (5.33)$$

### 5.2.4 The radial flow rate

$$WRFW = \sum_m \eta \nu^{m+2} G_m \quad (5.34)$$

$$G_m = \sum_n \eta^n d_{nm} (R_{nm}^{(11)} - R_{nm}^{(10)} + R_{nm}^{(00)} - R_{nm}^{(01)}) \quad (5.35)$$

$$R_{nm}^{(ij)} = \int_{-1}^{+1} \int_{-1}^{+1} \frac{u^n v^m}{3} \left( \frac{1}{\nu} \arctan\left(\frac{Z_i X_{ij}}{\nu(v+1)}\right) - \frac{(v+1)Z_i X_{ij}}{(\nu^2(v+1)^2 + Z_i^2)} \right) dudv \quad (5.36)$$

where:

$$X_{ij} = \sin\left(\arctan\left(\frac{x_j - \eta u}{\sqrt{\nu^2(v+1)^2 + Z_i^2}}\right)\right)$$

### 5.3 The East Face

After the appropriate transformations, the results for the east face are:

#### 5.3.1 The isotropic flow rate

$$EIFW = \sum_m (-1)^{m+3} \eta \nu^{m+2} G_m \quad (5.37)$$

$$G_m = \sum_n (-1)^n \eta^n a_{nm} (I_{nm}^{(11)} - I_{nm}^{(10)} + I_{nm}^{(00)} - I_{nm}^{(01)}) \quad (5.38)$$

$$I_{nm}^{(ij)} = \int_{-1}^{+1} \int_{-1}^{+1} \frac{u^n v^m (v+1)}{2\sqrt{\nu^2(v+1)^2 + Z_i^2}} \arctan\left(\frac{x_j + \eta u}{\sqrt{\nu^2(v+1)^2 + Z_i^2}}\right) dudv \quad (5.39)$$

#### 5.3.2 The cosinazimuthal flow rate

$$ECFW = \sum_m (-1)^{m+3} \eta \nu^{m+2} G_m \quad (5.40)$$

$$G_m = \sum_n (-1)^n \eta^n b_{nm} (C_{nm}^{(10)} - C_{nm}^{(11)} + C_{nm}^{(01)} - C_{nm}^{(00)}) \quad (5.41)$$

$$C_{nm}^{(ij)} = \int_{-1}^{+1} \int_{-1}^{+1} \frac{u^n v^m (v+1) dudv}{3\sqrt{\nu^2(v+1)^2 + (x_j + \eta u)^2 + Z_i^2}} \quad (5.42)$$

### 5.3.3 The sinazimuthal flow rate

$$ESFW = \sum_m (-1)^{m+4} \eta \nu^{m+3} G_m \quad (5.43)$$

$$G_m = \sum_n (-1)^n \eta^n c_{nm} (S_{nm}^{(10)} - S_{nm}^{(11)} + S_{nm}^{(01)} - S_{nm}^{(00)}) \quad (5.44)$$

$$S_{nm}^{(ij)} = \int_{-1}^{+1} \int_{-1}^{+1} \frac{u^n v^m (v+1)^2 (x_j + \eta u) dudv}{3(\nu^2(v+1)^2 + Z_i^2) \sqrt{\nu^2(v+1)^2 + (x_j + \eta u)^2 + Z_i^2}} \quad (5.45)$$

### 5.3.4 The radial flow rate

$$ERFW = \sum_m (-1)^{m+3} \eta \nu^{m+2} G_m \quad (5.46)$$

$$G_m = \sum_n (-1)^n \eta^n d_{nm} (R_{nm}^{(10)} - R_{nm}^{(11)} + R_{nm}^{(01)} - R_{nm}^{(00)}) \quad (5.47)$$

$$R_{nm}^{(ij)} = \int_{-1}^{+1} \int_{-1}^{+1} \frac{u^n v^m}{3} \left( \frac{1}{\nu} \arctan\left(\frac{Z_i X_{ij}}{\nu(v+1)}\right) - \frac{(v+1) X_{ij} Z_i}{\nu^2(v+1)^2 + Z_i^2} \right) dudv \quad (5.48)$$

where:

$$X_{ij} = \sin\left(\arctan\left(\frac{x_j + \eta u}{\sqrt{\nu^2(v+1)^2 + Z_i^2}}\right)\right)$$

## 5.4 The Top Face

### 5.4.1 The isotropic flow rate

$$TIFW = \sum_n (-1)^{n+3} \nu \eta^{n+2} G_n \quad (5.49)$$

$$G_n = \sum_m (-1)^m \nu^m a_{nm} (I_{nm}^{(11)} - I_{nm}^{(10)} + I_{nm}^{(00)} - I_{nm}^{(01)}) \quad (5.50)$$

$$I_{nm}^{(ij)} = \int_{-1}^{+1} \int_{-1}^{+1} \frac{u^n v^m (u+1)}{2\sqrt{\eta^2(u+1)^2 + Z_i^2}} \arctan\left(\frac{y_j + \nu v}{\sqrt{\eta^2(u+1)^2 + Z_i^2}}\right) dudv \quad (5.51)$$

#### 5.4.2 The cosinazimuthal flow rate

$$TCFW = \sum_n (-1)^{n+4} \nu \eta^{n+3} G_n \quad (5.52)$$

$$G_n = \sum_m (-1)^m \nu^m b_{nm} (C_{nm}^{(10)} - C_{nm}^{(11)} + C_{nm}^{(01)} - C_{nm}^{(00)}) \quad (5.53)$$

$$C_{nm}^{(ij)} = \int_{-1}^{+1} \int_{-1}^{+1} \frac{u^n v^m (u+1)^2 (y_j + \nu v) dudv}{3(\eta^2(u+1)^2 + Z_i^2) \sqrt{\eta^2(u+1)^2 + (y_j + \nu v)^2 + Z_i^2}} \quad (5.54)$$

#### 5.4.3 The sinazimuthal flow rate

$$TSFW = \sum_n (-1)^{n+3} \nu \eta^{n+2} G_n \quad (5.55)$$

$$G_n = \sum_m (-1)^m \nu^m c_{nm} (S_{nm}^{(10)} - S_{nm}^{(11)} + S_{nm}^{(01)} - S_{nm}^{(00)}) \quad (5.56)$$

$$S_{nm}^{(ij)} = \int_{-1}^{+1} \int_{-1}^{+1} \frac{u^n v^m (u+1) dudv}{3\sqrt{\eta^2(u+1)^2 + Z_i^2 + (y_j + \nu v)^2}} \quad (5.57)$$

#### 5.4.4 The radial flow rate

$$TRFW = \sum_n (-1)^{n+3} \nu \eta^{n+2} G_n \quad (5.58)$$

$$G_n = \sum_m (-1)^m \nu^m d_{nm} (R_{nm}^{(10)} - R_{nm}^{(11)} + R_{nm}^{(01)} - R_{nm}^{(00)}) \quad (5.59)$$

$$R_{nm}^{(ij)} = \int_{-1}^{+1} \int_{-1}^{+1} \frac{u^n v^m}{3} \left( \frac{1}{\eta} \arctan\left(\frac{Z_i X_{ij}}{\eta(u+1)}\right) - \frac{(u+1)X_{ij}Z_i}{\eta^2(u+1)^2 + Z_i^2} \right) dudv \quad (5.60)$$

where:

$$X_{ij} = \sin\left(\arctan\left(\frac{y_j + \nu v}{\sqrt{\eta^2(u+1)^2 + Z_i^2}}\right)\right)$$

## 5.5 The North Face

The transformation for the north face differs somewhat from the other faces since it occupies a position dissimilar to them. The major difference lies in the isotropic flow rate term for which an analytical solution of the integration over the window was not possible. However, an integration over one coordinate was successfully performed and a numerical quadrature was then used over the remaining three variables.

### 5.5.1 The isotropic flow rate

$$NIFW = 4\mu^2 Y^- \sum_n \eta^{n+1} G_n \quad (5.61)$$

$$G_n = \sum_m \nu^{m+1} a_{nm} (I_{nm}^{(1)} - I_{nm}^{(0)}) \quad (5.62)$$

$$I_{nm}^{(i)} = \int_{-1}^{+1} \int_{-1}^{+1} \int_{-1}^{+1} \frac{u^n v^m}{2A^2} \left( \frac{x_i - \eta u}{(x_i - \eta u)^2 + A^2} + \frac{1}{A} \arctan\left(\frac{x_i - \eta u}{A}\right) \right) dudvdw \quad (5.63)$$

where:

$$Y^- = \frac{(y_1 - y_0)}{2}$$

$$Y^+ = \frac{(y_1 + y_0)}{2}$$

$$A = \sqrt{(Y^- - w + Y^+ - \nu v)^2 + 4\mu^2}$$

### 5.5.2 The cosinazimuthal flow rate

$$NCFW = 4\mu^2 \sum_n \eta^{n+1} \nu G_n \quad (5.64)$$

$$G_n = \sum_m \nu^m b_{nm} (C_{nm}^{(10)} - C_{nm}^{(11)} + C_{nm}^{(01)} - C_{nm}^{(00)}) \quad (5.65)$$

$$C_{nm}^{(ij)} = \int_{-1}^{+1} \int_{-1}^{+1} \frac{u^n v^m (y_j - \nu v) dudv}{3((x_i - \eta u)^2 + 4\mu^2) \sqrt{(x_i - \eta u)^2 + 4\mu^2 + (y_j - \nu v)^2}} \quad (5.66)$$

### 5.5.3 The sinazimuthal flow rate

$$NSFW = 4\mu^2 \sum_n \eta^{n+1} \nu G_n \quad (5.67)$$

$$G_n = \sum_m \nu^m c_{nm} (S_{nm}^{(10)} - S_{nm}^{(11)} + S_{nm}^{(01)} - S_{nm}^{(00)}) \quad (5.68)$$

$$S_{nm}^{(ij)} = \int_{-1}^{+1} \int_{-1}^{+1} \frac{u^n v^m (x_i - \eta u) dudv}{3((y_j - \nu v)^2 + 4\mu^2) \sqrt{(x_i - \eta u)^2 + 4\mu^2 + (y_j - \nu v)^2}} \quad (5.69)$$

### 5.5.4 The radial flow rate

$$NRFW = 8\mu^3 \sum_n \nu \eta^{n+1} G_n \quad (5.70)$$

$$G_n = \sum_m \frac{\nu^m d_{nm}}{3} (R_{nm}^{(11)} - R_{nm}^{(10)} + R_{nm}^{(00)} - R_{nm}^{(01)}) \quad (5.71)$$

$$R_{nm}^{(ij)} = \int_{-1}^{+1} \int_{-1}^{+1} u^n v^m (F^{(ij)} + \frac{G^{(ij)}}{8\mu^3}) dudv \quad (5.72)$$

where:

$$F^{(ij)} = \frac{\omega_i(\omega_i^2 + 8\mu^2 - 4\mu^2 X_{ij}^2)X_{ij}}{4\mu^2(\omega_i^2 X_{ij}^2 + 4\mu^2)(\omega_i^2 + 4\mu^2)}$$

$$G^{(ij)} = \arctan\left(\frac{\omega_i X_{ij}}{2\mu}\right)$$

and:

$$\omega_i = x_i - \eta u$$

$$X_{ij} = \sin\left(\arctan\left(\frac{y_j - \nu v}{\sqrt{(x_i - \eta u)^2 + 4\mu^2}}\right)\right)$$

## 6. NEUTRON BALANCE(A BENCHMARK PROBLEM)

### 6.1 The Numerical Quadrature

To solve for the double and triple integrals that arise in the flow rate expressions (Chapter 5) a numerical quadrature was used. Subroutines D01DAF [12] and D01FCF [13] were called from the NAG fortran library.

D01DAF attempts to evaluate a double integral to a specified absolute accuracy by repeated applications of the method described by Patterson [14]. This routine attempts to evaluate a definite integral of the form

$$I = \int_a^b \int_{\varphi_1(y)}^{\varphi_2(y)} f(x, y) dx dy \quad (6.1)$$

where a and b are constants and  $\varphi_1(y)$  and  $\varphi_2(y)$  are functions of the variable y.

The integral is evaluated by expressing it as

$$I = \int_a^b F(y) dy$$

where

$$F(y) = \int_{\varphi_1(y)}^{\varphi_2(y)} f(x, y) dx$$

Both the outer integral I and the inner integrals F(y) are evaluated by the method described by Patterson, of the optimum addition of points to Gauss quadrature formulae.

This method uses a family of interlacing common point formulae. Beginning with the 3 point Gauss rule, formulae using 7, 15, 31, 63, 127, and finally 255 points are derived. Each new formula contains all the pivots of the earlier formulae so that no function evaluations are wasted. Each integral is evaluated by applying these formulae successively until two results are obtained which differ by less than the specified absolute accuracy.

D01FCF attempts to evaluate a multidimensional integral (up to 15 dimensions) with constant and finite limits, to a specified accuracy, using an adaptive division strategy. The routine operates by repeated subdivision of the hyper-rectangular region into smaller hyper-rectangles. In each subregion, the integral is estimated using a seventh degree rule, and an error estimate is obtained by comparison with a fifth-degree rule which uses a subset of the same points. The fourth differences on the integrand along each coordinate axis are evaluated, and the subregion is marked for possible future subdivision in half along that coordinate axis which has the largest absolute fourth difference. D01FCF is based on the HALF subroutine developed by Van Dooren and De Ridder [15]. It uses a different basic rule, described by Genz and Malik [16].

An alternate numerical integration program is provided in APPENDIX B. This program uses a Legendre-Gauss quadrature which work as follow.

For a single integral:

$$\int_{-1}^{+1} f(x)dx \simeq \sum_{i=1}^n H_i f(x_i)$$

For a double integral:

$$\int_{-1}^{+1} \int_{-1}^{+1} f(x, y) dx dy \simeq \sum_{i=1}^n \sum_{j=1}^m H_{ij} f(x_i, y_j)$$

For a triple integral:

$$\int_{-1}^{+1} \int_{-1}^{+1} \int_{-1}^{+1} f(x, y, z) dx dy dz \simeq \sum_{i=1}^n \sum_{j=1}^m \sum_{k=1}^l H_{ijk} f(x_i, y_j, z_k)$$

where  $H_i$ ,  $H_{ij}$ ,  $H_{ijk}$  are the weighting coefficients.

It goes without saying that the user might want to write his/her own numerical code. For this purpose he/she might want to use a numerical quadrature on only a single integral, for his/her convenience the appropriate reduced formulas are provided in APPENDIX A.

## 6.2 Neutron Balance

Since there must not be an accumulation or loss of neutrons inside the void, the number of neutrons per second that enters the void through the source face must be equal to the number of neutrons per second that exits from all five other faces.

This neutron conservation principle provides a benchmark problem to test the validity of the flow rate expressions.

The following "sample problem" has been chosen:

$$\eta = 1.0$$

$$\nu = 1.0$$

$$\mu = 2.0$$

$$\phi_0(x, y, z) = 3 - \left( \frac{x^2}{\eta^2} + \frac{y^2}{\nu^2} + \frac{z^2}{\mu^2} \right)$$

$$(6.2)$$

After using Eq. (3.2), Eq. (3.3) and Eq. (3.4) with  $D=1/3$  and setting  $z = -2$  one has:

$$\Phi_0(x, y) = 2 - (x^2 + y^2) \quad (6.3)$$

$$\Phi_1(x, y) = 2x \quad (6.4)$$

$$\Phi_2(x, y) = 2y \quad (6.5)$$

$$\Phi_3(x, y) = -1.0 \quad (6.6)$$

### 6.2.1 The incoming flow rate

The incoming flow rate (IFW) is the number of neutrons per second that enters the void through the source face. It can be computed through:

$$IFW = \int_s \int_{2\pi^+} \varphi_s(x, y, \theta, \psi) \cos \theta \, dS \, d\Omega \quad (6.7)$$

since

$$d\Omega = \sin \theta \, d\theta \, d\psi$$

then

$$IFW = \int_0^{2\pi} d\psi \int_0^{\frac{\pi}{2}} \cos \theta \sin \theta \, d\theta \int_s \varphi_s(x, y, \theta, \psi) \, dx \, dy \quad (6.8)$$

Replacing  $\varphi_s$  by its expansion Eq. (3.5), we can see that there are four contributions due to the components of the angular flux.

**The isotropic contribution:** Using Eq. (6.3) one has

$$IFW^{(i)} = \int_0^{2\pi} d\psi \int_0^{\frac{\pi}{2}} \cos \theta \sin \theta \, d\theta \int_s (2 - x^2 - y^2) \, dx \, dy \quad (6.9)$$

which yields

$$IFW^{(i)} = 16.755161$$

**The cosinazimuthal contribution:** Using Eq. (6.4) one has

$$IFW^{(c)} = \int_0^{2\pi} \cos \psi d\psi \int_0^{\frac{\pi}{2}} \cos \theta \sin^2 \theta d\theta \int_s 2x dx dy \quad (6.10)$$

which gives:

$$IFW^{(c)} = 0.0$$

**The sinazimuthal contribution:** Using Eq. (6.5) one has

$$IFW^{(s)} = \int_0^{2\pi} \sin \psi d\psi \int_0^{\frac{\pi}{2}} \cos \theta \sin^2 \theta d\theta \int_s 2y dx dy \quad (6.11)$$

which gives

$$IFW^{(s)} = 0.0$$

**The radial contribution:** Using Eq. (6.6) one has

$$IFW^{(r)} = \int_0^{2\pi} d\psi \int_0^{\frac{\pi}{2}} \cos^2 \theta \sin \theta d\theta \int_s (-1.0) dx dy \quad (6.12)$$

which gives:

$$IFW^{(r)} = -8.377580$$

It is now possible to obtain a numerical value for the total incoming flow rate by adding the four contributions:

$$IFW = IFW^{(i)} + IFW^{(c)} + IFW^{(s)} + IFW^{(r)}$$

$$IFW = 8.3775810$$

### 6.2.2 The outcoming flow rate

The outcoming flow rate (OFW) is the number of neutrons per second that exits from the void. It can be computed through the use of the flow rate expressions derived in Chapter 5, where the “window” was extended to the whole face. A computer program has been written for this purpose. An output of the program is detailed in Table 6.1 and Table 6.2. Table 6.2 clearly shows that the neutron balance is met, i.e., IFW=OFW.

The number of significant figures listed in the table are not necessary for a practical problem but were used to show the accuracy of the numerical integration.

Table 6.1: Flow rates components across the faces of the void for the sample problem

faces	isotropic	cosinaz.	sinaz.	radial
bottom	3.897559	0.5496408	-0.4886701	-1.886308
west	3.897559	-0.4886701	0.5496408	-1.886308
east	3.897559	-0.4886701	0.5496408	-1.886308
top	3.897559	0.5496408	-0.4886701	-1.886308
north	1.1649267	-0.1219414	-0.1219414	-0.8323495
total	16.7551627	0.0000000	0.0000000	-8.3775815

Table 6.2: Total Flow rates across the faces of the void for the sample problem

faces	flow rates
bottom	2.0722217
west	2.0722217
east	2.0722217
top	2.0722217
north	0.0886944
total (OFW)	8.3775812
void input (IFW)	8.3775810

## 7. GENERAL EQUATIONS(CONCEPT OF TRANSFER MATRIX)

The analysis carried out in the previous chapters assumes that only one face is a source of neutrons, however for a realistic problem one must take into account the fact that neutrons are streaming into the void, in general, from all its six faces. The logical steps to follow now, would be to switch the source to a new position and rederive the flow rate expressions for the five remaining faces. However, this routine approach is rather lengthy and tedious. Therefore we have developed the concept of a transfer matrix, which will simplify our task. A similar technique has been developed for nodes with neutron transport through materials called the response matrix method [17].

### 7.1 The Transfer Matrix

The transfer matrix comes into play when one needs to take into account the fact that neutrons will be streaming into the void from all faces of the void or at least from more than one face. The concept of a transfer matrix is best illustrated if we consider the following problem:

Assume that all six faces of the void are sources and in each face there is a window so that the total number of windows is also six. Consider now a single window, the total flow rate of neutrons streaming outbound through it will be the sum of the contributions incoming from the five surrounding source faces. Hence, a complete

solution consists of finding the total outbound flow rate across each of the six windows.

We will start by constructing the transfer matrix associated with this problem.

### 7.1.1 Definition of the transfer matrix

If we consider the south face of the void (which is source of neutrons), we can apply the results derived in Chapter 5, to find the outbound flow rates across the five windows located respectively in the bottom, top, east, west and north faces of the void. The transfer matrix  $\underline{A}_t$  associated with the void can then be defined such that it operates on matrix column  $\tilde{C}$  and produces matrix column  $\tilde{F}$ , where the entries of  $\tilde{F}$  are just the components<sup>1</sup> of the flow rates across the five windows surrounding the south face and the entries of  $\tilde{C}$  are the expansion coefficients  $a_{nm}, b_{nm}, c_{nm}$  or  $d_{nm}$  (relative to the south face), arranged in a chosen<sup>2</sup> order.

$$\tilde{F} = \underline{A}_t \cdot \tilde{C} \quad (7.1)$$

Consequently, it is clear that a transfer matrix is needed for each component so that four transfer matrices needs to be constructed.

If the other faces are sources, similar treatments can be used by multiplying the transfer matrix  $\underline{A}_t$  by a matrix column whose entries are the expansion coefficients relative to the appropriate face; the results are the sought flow rates.

---

<sup>1</sup>Isotropic, cosinazimuthal, sinazimuthal or radial.

<sup>2</sup>The arrangement of those entries is a free choice.

### 7.1.2 Construction of the transfer matrix

The transfer matrix is a  $I \times J$  matrix, where  $I$  is the number of windows across which the neutron flow rates are sought and  $J$  is the number of expansion coefficients in the polynomial formulation of the spatial fluxes (see relations (3.6) through (3.9)).

The transfer matrix for a particular component<sup>3</sup> can be constructed in the following manner:

first column:

Let the first expansion coefficient (e.g.,  $a_{00}$ ) be equal to unity and all others be equal to zero then seek the flow rates of that particular component across the windows through the use of expressions found in Chapter 5. These flow rates would then be the entries of the first column of the transfer matrix.

second column:

Let the second expansion coefficient (e.g.,  $a_{10}$ ) be equal to unity and all others be equal to zero and repeat the procedure described above. The entries of the second column will then be generated.

$i_{th}$  column:

Let the  $i_{th}$  expansion coefficient be equal to unity and all others be equal to zero and repeat the same steps.

It is now clear that, such a generated matrix, when multiplied by a matrix column containing the expansion coefficients will produce the neutron flow rates. The transfer matrix depends, of course, on the window coordinates and on the dimensions of the face.

---

<sup>3</sup>Isotropic, cosinazimuthal, sinazimuthal or radial.

Hence, for a cubical void, only a set of four matrices (one for each component) will be needed, whereas for a noncubical void three sets of four matrices need to be generated: one set will be used for the south and north faces, another set for the east and west faces and finally the last set for the bottom and top faces. When generating the transfer matrices, the dimensions of the void should be  $(\eta, \nu, \mu)$  for the south and north faces,  $(\eta, \mu, \nu)$  for the east and west faces and  $(\mu, \nu, \eta)$  for the bottom and top faces.

## 7.2 Use of the Transfer Matrix in the Nodal Model

In the nodal method, the nodes are coupled to each other through the neutron partial currents. These currents can be found by solving the diffusion equation in the node and using the appropriate boundary conditions. An existing void within the medium cannot, of course, be handled in a similar fashion. The transfer matrix model developed in this work provides the partial currents (at the boundaries) that couple the void to its surrounding nodes.

## 7.3 Benchmark Problem

We will again use the neutron balance as a benchmark problem. We will choose all six faces of the void to be sources and compare the total number of neutrons streaming into the void with the total number of neutrons streaming outbound through the six faces of the void. This conservation of neutrons principle should test the validity of the concept of the transfer matrix.

The void chosen will have the following dimensions:

$$\eta = 1.0$$

$$\nu = 1.0$$

$$\mu = 2.0$$

(7.2)

The isotropic component of the angular flux will be assumed to be the same on all six faces, i.e.:

$$\phi_0(x, y, z) = 3 - \left( \frac{x^2}{\eta^2} + \frac{y^2}{\nu^2} + \frac{z^2}{\mu^2} \right)$$

(7.3)

using relations (3.2) through (3.4), we find:

$$\begin{aligned} \phi_1(x, y, z) &= \frac{2x}{\eta^2} \\ \phi_2(x, y, z) &= \frac{2y}{\nu^2} \\ \phi_3(x, y, z) &= \frac{2z}{\mu^2} \end{aligned}$$

(7.4)

where it was assumed that  $D=1/3$

The six angular fluxes may then be found to be:

$$\varphi_b(r, \hat{\Omega}) = 2 - \left( y^2 + \frac{z^2}{4} \right) - 2 \sin \theta \cos \psi + 2y \sin \theta \sin \psi + 0.5z \cos \theta \quad (7.5)$$

$$\varphi_t(r, \hat{\Omega}) = 2 - \left( y^2 + \frac{z^2}{4} \right) + 2 \sin \theta \cos \psi + 2y \sin \theta \sin \psi + 0.5z \cos \theta \quad (7.6)$$

$$\varphi_e(r, \hat{\Omega}) = 2 - \left( x^2 + \frac{z^2}{4} \right) + 2x \sin \theta \cos \psi + 2 \sin \theta \sin \psi + 0.5z \cos \theta \quad (7.7)$$

$$\varphi_w(r, \hat{\Omega}) = 2 - \left(x^2 + \frac{z^2}{4}\right) + 2x \sin \theta \cos \psi - 2 \sin \theta \sin \psi + 0.5z \cos \theta \quad (7.8)$$

$$\varphi_n(r, \hat{\Omega}) = 2 - (x^2 + y^2) + 2x \sin \theta \cos \psi + 2y \sin \theta \sin \psi + \cos \theta \quad (7.9)$$

$$\varphi_s(r, \hat{\Omega}) = 2 - (x^2 + y^2) + 2x \sin \theta \cos \psi + 2y \sin \theta \sin \psi - \cos \theta \quad (7.10)$$

The subscripts b, t, e, w, n and s stands for bottom, top, east, west, north and south respectively.

### 7.3.1 The incoming flow rate (IFW)

Eq. (6.7) applied to each face gives the number of neutrons entering the void through the corresponding face, the angular fluxes are given by Eq. (7.5) through Eq. (7.10).

The integration when performed leads to the following results:

Table 7.1: Inbound neutron flow rates across faces of the void

faces	isotropic	cosinaz.	sinaz.	radial
bottom	33.5103216	0.0000000	0.0000000	0.0000000
west	33.5103216	0.0000000	0.0000000	0.0000000
east	33.5103216	0.0000000	0.0000000	0.0000000
south	16.7551610	0.0000000	0.0000000	-8.3775810
north	16.7551610	0.0000000	0.0000000	8.3775810
top	33.5103216	0.0000000	0.0000000	0.0000000

The total number of neutrons (IFW) entering the void can then be obtained by summing over all the faces:

$$IFW = 167.5516096$$

### 7.3.2 The outcoming flow rate (OFW)

A computer program has been written to generate the 12 Transfer Matrices for this problem. A subroutine has also been written to multiply the transfer matrices by the appropriate column matrices containing the expansion coefficients. The results which are the neutron flow rates streaming out across the faces of the void are detailed in Tables (7.2) through (7.14). Table (7.14) contains the total neutron flow rate crossing outbound each face and the total neutron flow rate (OFW) that exits from the void.

The total outbound flow rate OFW, when compared against the total neutron flow rate (IFW) that enters the void through all six faces, satisfy the neutron balance (i.e.,  $OFW=IFW$ ).

Table 7.2: Flow rates components across faces of the void when the top face is the only source

faces	isotropic	cosinaz.	sinaz.	radial
bottom	10.046688	0.0000000	-1.4232648	0.0000000
west	8.1158200	0.0000000	1.2052664	0.0000000
east	8.1158200	0.0000000	1.2052664	0.0000000
south	3.6156136	-3.7672896	-0.5179087	0.9797506
north	3.6156136	3.7672896	-0.5179087	-0.9797506

Table 7.3: Total Flow rates across faces of the void when the top face is the only source

faces	flow rates
bottom	8.6234232
west	9.3210864
east	9.3210864
south	0.3101659
north	5.8852439

Table 7.4: Flow rates components across faces of the void when the bottom face is the only source

faces	isotropic	cosinaz.	sinaz.	radial
top	10.046688	0.0000000	-1.4232648	0.0000000
west	8.1158200	0.0000000	1.2052664	0.0000000
east	8.1158200	0.0000000	1.2052664	0.0000000
south	3.6156136	3.7672896	-0.5179087	-0.9797506
north	3.6156136	-3.7672896	-0.5179087	0.9797506

Table 7.5: Total Flow rates across faces of the void when the bottom face is the only source

faces	flow rates
top	8.6234232
west	9.3210864
east	9.3210864
north	0.3101659
south	5.8852439

Table 7.6: Flow rates components across faces of the void when the east face is the only source

faces	isotropic	cosinaz.	sinaz.	radial
top	8.1162650	1.2012244	0.0000000	0.0000000
west	10.046688	-1.4207576	0.0000000	0.0000000
bottom	8.1162650	1.2012244	0.0000000	0.0000000
south	3.6161744	-0.5284805	-3.7845964	0.9841580
north	3.6161744	-0.5284805	3.7845964	-0.9841580

Table 7.7: Total Flow rates across faces of the void when the east face is the only source

faces	flow rates
top	9.3174894
west	8.6259304
bottom	9.3174894
north	5.8881323
south	0.2872555

Table 7.8: Flow rates components across faces of the void when the west face is the only source

faces	isotropic	cosinaz.	sinaz.	radial
top	8.1162650	1.2012244	0.0000000	0.0000000
east	10.046688	-1.4207576	0.0000000	0.0000000
bottom	8.1162650	1.2012244	0.0000000	0.0000000
south	3.6161744	-0.5284805	-3.7845964	0.9841580
north	3.6161744	-0.5284805	3.7845964	-0.9841580

Table 7.9: Total Flow rates across faces of the void when the west face is the only source

faces	flow rates
top	9.3174894
bottom	9.3174894
east	8.6259304
north	5.8881323
south	0.2872555

Table 7.10: Flow rates components across faces of the void when the north face is the only source

faces	isotropic	cosinaz.	sinaz.	radial
bottom	3.897559	0.5496408	-0.4886701	1.8863632
west	3.897559	-0.4886701	0.5496408	1.8863632
east	3.897559	-0.4886701	0.5496408	1.8863632
top	3.897559	0.5496408	-0.4886701	1.8863632
south	1.1649267	-0.1219414	-0.1219414	0.8323740

Table 7.11: Total Flow rates across faces of the void when the north face is the only source

faces	flow rates
bottom	5.8448929
west	5.8448929
east	5.8448929
top	5.8448929
south	1.7534179

Table 7.12: Flow rates components across faces of the void when the south face is the only source

faces	isotropic	cosinaz.	sinaz.	radial
bottom	3.897559	0.5496408	-0.4886701	-1.8863632
west	3.897559	-0.4886701	0.5496408	-1.8863632
east	3.897559	-0.4886701	0.5496408	-1.8863632
top	3.897559	0.5496408	-0.4886701	-1.8863632
south	1.1649267	-0.1219414	-0.1219414	-0.8323740

Table 7.13: Total Flow rates across faces of the void when the south face is the only source

faces	flow rates
bottom	2.0722217
west	2.0722217
east	2.0722217
top	2.0722217
north	0.0886944

Table 7.14: Total Flow rates across faces of the void (all faces being sources)

faces	flow rates
bottom	33.461006
west	33.436297
east	33.436297
top	33.461006
south	8.3775812
north	25.1329895
total(OFW)	167.3051767

## 8. THE OVERALL TRANSFER MATRIX

In the nodal method, the spatial neutron flux distribution within a node is generally expressed in terms of the Legendre polynomials [10]:

$$\phi(u, v, w) = \sum_n \sum_m \sum_l a_{nml} P_n(u) P_m(v) P_l(w) \quad (8.1)$$

where

$$u = \frac{x}{\eta}, v = \frac{y}{\nu}, w = \frac{z}{\mu}$$

and  $P_n(u)$ ,  $P_m(v)$ ,  $P_l(w)$  are Legendre polynomials.

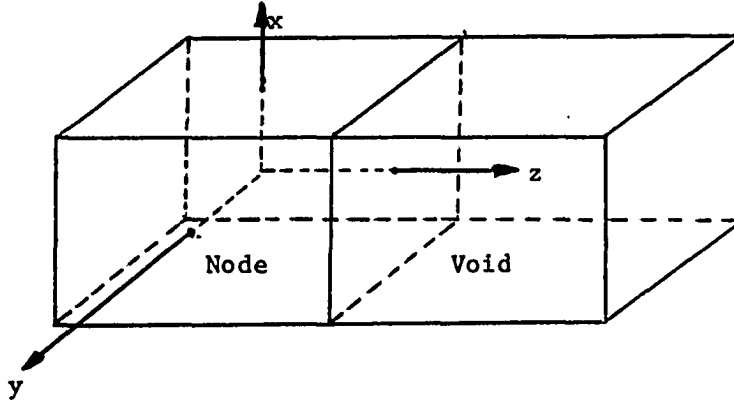


Figure 8.1: A void and its adjacent node

The coordinate system  $(x,y,z)$  has its center located at the center of the node and  $\eta$ ,  $\nu$ ,  $\mu$  are the node dimensions assumed to be the same as the adjacent void dimensions (see Figure 8.1). Since the regular polynomial formulation of the spatial

neutron flux is used in this work rather than the Legendre polynomials, we need to convert the coefficients  $a_{nml}$  of Eq. (8.1) to their corresponding polynomial expansion coefficients. This can easily be done through a transformation matrix [2].

Let  $\underline{l}^{(3)}$  be the matrix column whose entries are the Legendre expansion coefficients and  $\underline{p}^{(3)}$  be the matrix whose entries are the corresponding polynomial expansion coefficients. We will then define the matrix  $L_g$  to be the matrix which transform the Legendre coefficients to the polynomial coefficients:

$$\underline{p}^{(3)} = L_g \cdot \underline{l}^{(3)} \quad (8.2)$$

The entries of  $\underline{p}^{(3)}$  are three indices coefficients (i.e.,  $a_{nml}$ ) which describe the neutron flux polynomial expansion in the node volume. Thus, since the transfer matrix model uses a flux distribution on a surface, we need to convert these coefficients to two-index coefficients (i.e.,  $a_{nm}$ ) as required by relations (3.6) through (3.9). This can be done by setting  $w=1.0$  in Eq. (8.1) or using a transformation matrix [2].

Let  $B_0$ ,  $B_1$ ,  $B_2$  and  $B_3$  be the matrices, that convert the three-dimensional coefficients to the two-dimensional coefficients, for the isotropic, cosinazimuthal, sinazimuthal and radial components of the flux respectively. Then:

$$\underline{p}_0^{(2)} = B_0 \cdot \underline{p}^{(3)} \quad (8.3)$$

$$\underline{p}_1^{(2)} = B_1 \cdot \underline{p}^{(3)} \quad (8.4)$$

$$\underline{p}_2^{(2)} = B_2 \cdot \underline{p}^{(3)} \quad (8.5)$$

$$\underline{p}_3^{(2)} = B_3 \cdot \underline{p}^{(3)} \quad (8.6)$$

where subscripts 0, 1, 2, 3 stands for isotropic, cosinazimuthal, sinazimuthal and radial respectively and superscripts (2) and (3) stands for two dimensions and three

dimensions respectively.

The neutron partial currents (in matrix formulation) can now be obtained by multiplying the transfer matrices by the two-dimensional coefficients matrices:

$$\underline{j}_0 = T_0 \cdot \underline{p}_0^{(2)} \quad (8.7)$$

$$\underline{j}_1 = T_1 \cdot \underline{p}_1^{(2)} \quad (8.8)$$

$$\underline{j}_2 = T_2 \cdot \underline{p}_2^{(2)} \quad (8.9)$$

$$\underline{j}_3 = T_3 \cdot \underline{p}_3^{(2)} \quad (8.10)$$

where  $\underline{j}_0$ ,  $\underline{j}_1$ ,  $\underline{j}_2$  and  $\underline{j}_3$  are the isotropic, cosinazimuthal, sinazimuthal and radial components of the neutron partial current and  $T_0$ ,  $T_1$ ,  $T_2$  and  $T_3$  are the transfer matrices associated with this components.

The net partial current is then:

$$\underline{j}_{net} = \underline{j}_0 + \underline{j}_1 + \underline{j}_2 + \underline{j}_3 \quad (8.11)$$

Making use of relations (8.2) through (8.10) one has:

$$\underline{j}_{net} = ((T_0 B_0 + T_1 B_1 + T_2 B_2 + T_3 B_3) \cdot L_g) \cdot \underline{l}^{(3)} \quad (8.12)$$

the matrix:

$$T = (T_0 B_0 + T_1 B_1 + T_2 B_2 + T_3 B_3) \cdot L_g$$

is called the overall transfer matrix, and the relation:

$$\underline{j}_{net} = T \cdot \underline{l}^{(3)} \quad (8.13)$$

is called the void equation.

It can be shown [2] that the number of operations performed to obtain the neutron partial currents by using the overall transfer matrix is significantly less than if the simple transfer matrices defined earlier are used. This feature makes the overall transfer matrix a desirable tool to work with. For a void with fixed size and fixed window coordinates the overall transfer matrix is unique and the void equation relates quite simply the flux distribution in the adjacent node to the outbound partial currents that couple the void to its surrounding nodes.

An alternate way of constructing the overall transfer matrix, which has a definite advantage over the one previously described in that the matrices involved are independent of the neighboring node dimensions, starts by converting the three-indices Legendre coefficients (i.e.,  $a_{nml}$ ) to the two-index Legendre coefficients (i.e.,  $a_{nm}$ ) over the interface between the void and the neighboring node:

$$l^{(2)} = C.l^{(3)} \quad (8.14)$$

$C$  is the transformation matrix. The two-index Legendre coefficients are now converted into the two-index polynomial coefficients through:

$$p_0^{(2)} = B_0.l^{(2)} \quad (8.15)$$

$$p_1^{(2)} = B_1.l^{(2)} \quad (8.16)$$

$$p_2^{(2)} = B_2.l^{(2)} \quad (8.17)$$

$$p_3^{(2)} = B_3.l^{(2)} \quad (8.18)$$

$B_0$ ,  $B_1$ ,  $B_2$  and  $B_3$  are the appropriate transformation matrices. The neutron partial currents (in matrix formulation) can now be obtained by multiplying the

transfer matrices by the two-dimensional coefficients matrices:

$$\underline{j}_0 = T_0 \cdot \underline{p}_0^{(2)} \quad (8.19)$$

$$\underline{j}_1 = T_1 \cdot \underline{p}_1^{(2)} \quad (8.20)$$

$$\underline{j}_2 = T_2 \cdot \underline{p}_2^{(2)} \quad (8.21)$$

$$\underline{j}_3 = T_3 \cdot \underline{p}_3^{(2)} \quad (8.22)$$

where  $\underline{j}_0$ ,  $\underline{j}_1$ ,  $\underline{j}_2$  and  $\underline{j}_3$  are the isotropic, cosinazimuthal, sinazimuthal and radial components of the neutron partial current and  $T_0$ ,  $T_1$ ,  $T_2$  and  $T_3$  are the transfer matrices associated with this components.

The overall transfer matrix is then:

$$T = T_0 B_0 C_0 + T_1 B_1 C + T_2 B_2 C + T_3 B_3 C$$

## 9. MODEL LIMITATIONS

Values of the diffusion coefficient found in the present generation of nuclear reactors are in the 0.1-2 cm range [18]. The present model when used in conjunction with the multigroup analysis spans completely this range. For each group ( $g$ ) we can associate a corresponding group diffusion coefficient  $D_g$  and apply the transfer matrix model. Sizes of the node in the nodal method are in the 10-20 cm range [17] and are then compatible with the units of the diffusion coefficient.

The limitations of this model, beyond the fact that the P1 approximation is used, arise when it is applied to the "Flat" void and to the "Long" void configurations which are shown in Figure 9.1 and in Figure 9.2.

In the "Flat" void, one side is much smaller than the other two (e.g.,  $\mu \ll \eta, \nu$ ) and in the "Long" void two sides are much smaller than the third one (e.g.,  $\mu \gg \eta, \nu$ ).

For a sufficiently thin "Flat" void and a "Long" void in which one dimension is much larger than the others, the neutron balance is not satisfied, indicating that the model is not applicable.

A computer program was written to determine the limiting dimensions beyond which the numerical quadrature for the model may fail. For the "Flat" void  $\eta$  and  $\nu$  have been equated to 10.0 cm and  $\mu$  has been decreased from a value of 4.0 cm to 0.5 cm (see Table 9.1). For this last value the relative error on the neutron balance

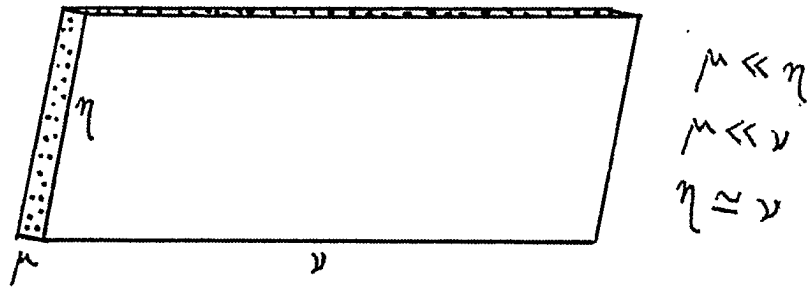


Figure 9.1: A Flat void

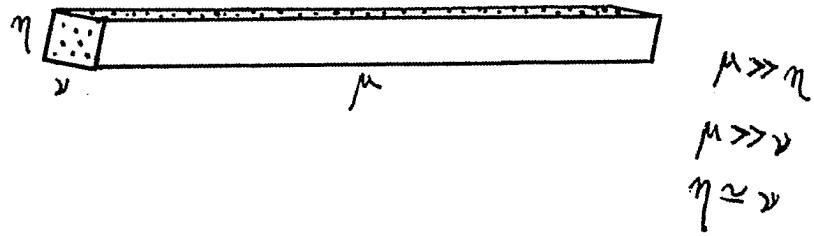


Figure 9.2: A Long void

has been found to be 0.15 % which has been chosen to be the limiting value. It is also viewed that voids this small would not be important in nodal models. For the "Long" void 0.75 cm has been found to be the limiting dimension (see Table 9.2).

Table 9.1: "Flat" void limiting dimension ( $\eta = \nu = 10.0$ )

$\mu$	IFW	OFW	relative neutron balance
2.0	5026.548	5028.715	0.04311 %
1.5	5305.800	5308.832	0.05714 %
1.2	5585.053	5588.004	0.05284 %
0.5	7539.821	7551.196	0.15000 %

Table 9.2: "Long" void limiting dimension ( $\nu = 10.0$ )

$\mu, \eta$	IFW	OFW	relative neutron balance
3.0	1424.189	1424.359	0.01200 %
1.0	586.4305	586.4637	0.00600 %
0.75	481.7109	482.3830	0.14000 %
0.5	376.9911	375.6801	0.34700 %

We reached now a point where the following conclusions may be drawn about the extreme void sizes:

(1) This model is inapplicable to a "Flat" void having the thin edge much less than 5 % of the smallest side of the two larger sides.

(2) It is not recommended to use this model for a "Long" void for which the larger side is over 13 times larger than the smallest side.

A computer program to test the model's applicability is provided in APPENDIX C. When dealing with special void configurations, one can use this test prior to using this model.

## 10. SUMMARY AND CONCLUSIONS

### 10.1 Summary

Using a "radiation like" treatment of the streaming of neutrons inside a void, we have been successful in building a model for the P1 neutron approximation that enables one to predict the neutron current ( $J$ ) that exits from a "window" located in any face of a rectangular cavity. This neutron partial current can hence be coupled with an adjacent node for use within the nodal method. The streaming is developed in terms of entries in a transfer matrix which can be applied to polynomial coefficients for the neutron flux on one source face of a rectangular void. A favorable point for this model is that it avoids the complexity of using the neutron transport equation [1], or all its affiliated approximations, inside the void. To use this model, it is only required that the angular fluxes on the source faces are known in the form of polynomial expansion coefficients.

The model proceeds by evaluating double and triple integrals using a numerical quadrature and it must be said that widely available computer programs (for numerical integration) in the math library offers a variety of ways to do so.

Finally, this model aims to create the overall transfer matrix associated with a void, from this matrix many physical quantities can be inferred.

## 10.2 Special Comments

(1) In all computer programs that have been used in this analysis, either to check the neutron balance or to produce the transfer matrices, a call has been made to the NAG Library (Math Library for Numerical Algorithms). Subroutines D01DAF [12] and D01FCF [13] were used to compute double integrals and triple integrals respectively.

It has been observed that the NAG subroutines fails <sup>1</sup> for certain "class" of windows or for particular void's configurations. The reason is that when the usual  $10^{-6}$  accuracy is requested, the NAG subroutine uses 255 points for the numerical integration process and gives back a failure message if the two or three single integrals have still not converged. The remedy for this is to lower the requested accuracy until convergence is achieved. In certain instances, the accuracy had to be lowered to  $10^{-1}$  for acceptance by the NAG subroutines.

Since diffusion theory is used for this analysis, it would be irrelevant to request a  $10^{-6}$  on the integrals evaluation. An accuracy of  $10^{-2} - 10^{-3}$  should be sufficient. For the interested reader's convenience, a numerical integration program has been provided in APPENDIX B. This program would not experience failures and can evaluate integrals with accuracies within the above range.

The use of the NAG subroutines or other high-accuracy numerical codes may be deferred until later when the present model will be improved through the use of the  $P_N$  equations.

---

<sup>1</sup>The phenomenon is thought to be due to badly behaved integrands and has been observed to occur when either the void is small in size or when windows have at least a small side.

(2) All numerical integration codes usually require that the integrands do not experience singularities at points used in the numerical process. The user must be warned that the integrands that appears in the flow rates expressions derived in Chapter 5 exhibit such a singular behavior in some particular situations. Such situations occur when  $Z_i$  is equal to zero. Recall that since  $Z_i = z_i + \mu$  then windows for which  $z_i = -\mu$  may lead to integrand's singularities ( $Z_i = 0$  is a necessary but not sufficient condition, as will be shown below). Fortunately, those singularities are "removables" and a condition statement within the program does so.

A proof for removal of the singularity is shown in the example below. Consider  $S_{nm}^{(ij)}$ (bottom face):

$$S_{nm}^{(ij)} = \int_{-1}^{+1} \int_{-1}^{+1} \frac{u^n (u+1)v^m dudv}{3\sqrt{\eta^2(u+1)^2 + Z_i^2 + (y_j - \nu v)^2}} \quad (10.1)$$

It can be seen that the integrand will be singular when simultaneously:

$$\begin{aligned} Z_i &= 0 \\ u &= -1 \\ v &= \frac{y_j}{\nu} \end{aligned} \quad (10.2)$$

Actually when the above conditions are met and limits are taken

$$S_{nm}^{(ij)} = \int_{-1}^{+1} \int_{-1}^{+1} \frac{u^n v^m dudv}{3\eta} \quad (10.3)$$

Hence, a condition statement can be incorporated within the program to avoid a failure of the numerical quadrature. For all other integrals, the singularities are "removables".

### 10.3 Conclusions

The transfer matrix model developed in this analysis, which permits accounting for voids occupying nodal positions within the nodal model, has been established for the P1 neutron distribution. The theory is in agreement with the benchmarked neutron balance to better than 0.1%. In the nodal method, the size of the nodes is within the 10-20 cm range [17], and for such dimensions the model has been demonstrated to have the accuracy required. Its limitations would only be of concern for the "flat" and "long" configurations. It has been shown that for a "flat" void, the model is not applicable if the thin edge is much less than 5% of the smallest side of the two larger sides, the same thing can be said about a "long" void for which the larger side is over 13 times larger than the smallest side. The major contribution of the model built in this analysis is to introduce and compute the overall transfer matrix associated with a rectangular void. This matrix operates on a matrix associated with the neutron flux distribution in the adjacent node and produces the neutron partial currents, transferred from this node, which exit from the void through the chosen windows.

As research will progress in this area, it is expected that further applications of this transfer matrix will be brought into light; it may turn out to be a standard tool to solve void-related problems. The concept of the transfer matrix has already been proven useful when used within the nodal method [17].

## 11. SUGGESTIONS FOR FURTHER WORK

(1) The P1 Approximation used in this analysis assumes that the angular flux can be adequately represented by only a linearly anisotropic angular dependence [5]. As we know this assumption is inaccurate near boundaries or where material properties change dramatically across an interface and such a case can be seen to apply here, since neutrons would be streaming from an “active” media (adjacent node in the nodal method) to a “passive” media (void). Hence, it is desirable to try to improve the validity of this model by incorporating higher terms in the angular flux expansion ( $P_N$  equations). Further work then needs to be done which consists of evaluating additional integrals brought in by those higher components.

(2) Limiting cases for the void dimensions, i.e., “Flat” void and “Long” void (see Figures 9.1 and 9.2) results into further simplifications in the integration process which in turn would lead to substantial computational savings. The following example can clarify this matter:

For a “Long” void we know that:

$$\mu \gg \nu$$

$$\mu \gg \eta$$

If we are seeking the bottom sinazimuthal flow rate (BSFW), when the smallest face is source, we can write according to Eq. (5.20):

$$S_{nm}^{(ij)} = \int_{-1}^{+1} \int_{-1}^{+1} \frac{u^n (u+1) v^m dudv}{3\sqrt{\eta^2(u+1)^2 + Z_i^2 + (y_j - \nu v)^2}} \quad (11.1)$$

Now letting:

$$\eta \rightarrow 0$$

$$\nu \rightarrow 0$$

$$y_j \rightarrow 0$$

We obtain:

$$S_{nm}^{(ij)} \simeq \int_{-1}^{+1} \int_{-1}^{+1} \frac{u^n (u+1) v^m dudv}{3Z_i} \quad (11.2)$$

whose analytical solution is:

if m is odd

$$S_{nm}^{(ij)} \simeq 0$$

if m is even and n is odd

$$S_{nm}^{(ij)} \simeq \frac{4}{3Z_i(m+1)(n+2)}$$

if m is even and n is even

$$S_{nm}^{(ij)} \simeq \frac{4}{3Z_i(m+1)(n+1)}$$

Hence, we can see that for a “Long” void  $S_{nm}^{(ij)}$  (*bottom*) can be solved analytically.

A similar treatment of the other double integrals can be done for those limiting cases.

(3) The analysis that was carried on in this work applies only to a rectangular void geometry. Since voids can be spherical, cylindrical or can have other complex geometries in nature, it may be useful to derive similar flow rate expressions for such shapes.

(4) In the present work we have dealt only with one void. We may, however, encounter situations where two or more voids are accumulated next to each other (see Figure 11.1). It is desirable to investigate these cases.

Node	Node	Node	Node
Node	Void	Void	Node
Node	Node	Void	Node
Node	Node	Node	Node

Figure 11.1: An accumulation of three voids

(5) Due to the "radiation like" nature of neutrons, this model can be extended to account for the streaming of photons (Gamma radiation) as well. Since no build up factors take place inside the void, it can be done with relative ease.

## ACKNOWLEDGEMENTS

I wish to express my sincere gratitude to my major professor Dr. A. F. Rohach for his dedicated guidance throughout the whole course of this research work.

I have greatly appreciated the helpful comments from Dr. B. I. Spinrad and from Dr. R. A. Danofsky.

I must acknowledge my colleagues graduate students Ramin Mikaili and David Roth for their helpful attitude.

Erica Harris from the computation center helped a great deal on the writing part of this document.

I am also very much indebted to the Algerian Ministry of Higher Education and to the cultural section of the Algerian Embassy for their financial support which made this work possible.

Finally and above all, I would like to dedicate this research to my wife Fouzia for her constant moral support and would like to thank my daughter Hinda for helping us enjoy our stay in Ames.

## 12. BIBLIOGRAPHY

- [1] R. T. Ackroyd, J. G. Issa and N. S. Riyait. *Treatment of Voids in Finite Element Transport Methods*. Annals of Nuclear Energy, 18, No.1/2 (1986): 85-89.
- [2] A. F. Rohach, Department of Nuclear Engineering, Iowa State university, *Private communication*, 1989.
- [3] M. R. Wagner and K. Koebke. *Progress in Nodal Reactor Analysis*. Atomkernenergie, Kerntechnik, 43, No.2 (1983):117-125.
- [4] H. W. Graves. *Evaluation of Coupling Coefficients in Nodal/Modal Analysis*. Annals of Nuclear Energy, 11, No.5 (1984):213-223.
- [5] J. J. Duderstadt and L. J. Hamilton. *Nuclear Reactor Analysis*. New York, NY: John Wiley & Sons, 1986.
- [6] J.H.Hubbell, R.L.Bach and J.C.Lamkin. *Radiation Field From a Rectangular Source*. JOURNAL OF RESEARCH of the National Bureau of Standards-C. Engineering and Instrumentation 64C, No.2 (April-June 1960): 121-138.
- [7] Int. Atom. Energy Agc. *Engineering Compendium on Radiation Shielding*. Vol. I. Springer-Verlag, New York, 1968.

- [8] D. J. Behrens. *The Effect of Holes in a Reacting Material on the Passage of Neutrons*. Proc. Phys. Soc. (London) 62 Series A (1949): 607.
- [9] P. Benoist. *Formulation Generale et Calcul Pratique du Coefficient de Diffusion Dans un Reseau Comportant des Cavites*. CEA-1354 (1959).
- [10] A. F. Rohach. *A Legendre polynomial nodal model for 3-D diffusion problems*. Annals of Nuclear Energy, 14, No.12 (1987):653-661.
- [11] S. M. Selby. *Standard Mathematical Tables*. 20<sup>th</sup> Edition. Cleveland, OH: The Chemical Rubber Co., 1972.
- [12] D01DAF. *A Quadrature Code for a Double Integral Evaluation using Patterson's Method*. NAG FORTRAN LIBRARY (Routine Document), MARK 13, Vol. 1 (1988).
- [13] D01FCF. *A Quadrature Code for a Multidimensional Integral Evaluation using Adaptive Strategy Division*. NAG FORTRAN LIBRARY (Routine Document), MARK 13, Vol. 1 (1988).
- [14] Patterson, T.N.L. *Math. Comp.* 22 (1968): 847-856 and 877-881.
- [15] P. Van Dooren, and L. De Ridder. *An Adaptive Algorithm for Numerical Integration over an N-dimensional cube*. J. Comp. Appl. Math. 2, No.3 (1976): 207-217.
- [16] A. C. Genz and A. A. Malik. *An Adaptive Algorithm for Numerical Integration over an N-dimensional Rectangular Region*. J. Comp. Appl. Math. 6 (1980): 295-302.

- [17] R. J. Stammers and M. J. Abbate. *Methods of Steady-State Reactor Analysis in Nuclear Design*. New York, NY: Academic Press, 1984.
- [18] P. F. Zweifel. *Reactor Physics*. New York, NY: Mc Graw-Hill, Inc, 1973.

#### Additional References

- A. B. Chilton, J. K. Shultis and R. E. Faw. *Principles of Radiation Shielding*. Englewood Cliffs, NJ: Prentice Hall, Inc., 1984.
- Int. Atom. Energy Agc. *Engineering Compendium on Radiation Shielding*. Vol. II. Springer-Verlag, New York, 1975.
- Int. Atom. Energy Agc. *Engineering Compendium on Radiation Shielding*. Vol. III Springer-Verlag, New York, 1970.
- C. Carter. *Streaming due to Holes in a Reactor*. AERE-R3367 (November, 1960).

### 13. APPENDIX A. DOUBLE INTEGRATION REDUCTION

The double integration that arises in the flow rates expressions derived in Chapter 5 can be reduced, in some cases<sup>1</sup>, to a single integration. These double integrals can be classified into four functionals:

The Isotropic Functional:

$$H_i(n, m, a, b, c) = \int_{-1}^{+1} \int_{-1}^{+1} \frac{u^n v^m (u+1)}{2\sqrt{a^2(u+1)^2 + Z_i^2}} \arctan\left(\frac{c-bv}{\sqrt{a^2(u+1)^2 + Z_i^2}}\right) dudv \quad (13.1)$$

The Azimuthal Functionals:

$$J_i(n, m, a, b, c) = \int_{-1}^{+1} \int_{-1}^{+1} \frac{u^n (u+1)^2 v^m (c-bv) dudv}{3(a^2(u+1)^2 + Z_i^2)\sqrt{a^2(u+1)^2 + (c-bv)^2 + Z_i^2}} \quad (13.2)$$

$$K_i(n, m, a, b, c) = \int_{-1}^{+1} \int_{-1}^{+1} \frac{u^n (u+1)v^m dudv}{3\sqrt{a^2(u+1)^2 + Z_i^2 + (c-bv)^2}} \quad (13.3)$$

$$L(n, m, a, b, c, d) = \int_{-1}^{+1} \int_{-1}^{+1} \frac{u^n v^m (d-bv) dudv}{3((c-au)^2 + 4\mu^2)\sqrt{(c-au)^2 + 4\mu^2 + (d-bv)^2}} \quad (13.4)$$

In the flow rates expressions (Chapter 5), we have encountered the double integrals  $I_{nm}^{(ij)}$ ,  $C_{nm}^{(ij)}$ ,  $S_{nm}^{(ij)}$  and  $R_{nm}^{(ij)}$  which can now easily be expressed in terms of the four

<sup>1</sup>No further reductions is possible for the north isotropic flow rate and for all radial flow rates.

functionals defined above.

It is easy to verify that:

$$\begin{aligned} I_{nm}^{(ij)}(\text{bottom}) &= H_i(n, m, \eta, \nu, y_j) \\ I_{nm}^{(ij)}(\text{west}) &= H_i(m, n, \nu, \eta, x_j) \\ I_{nm}^{(ij)}(\text{east}) &= H_i(m, n, \nu, -\eta, x_j) \\ I_{nm}^{(ij)}(\text{top}) &= H_i(n, m, \eta, -\nu, y_j) \end{aligned}$$

and that:

$$\begin{aligned} C_{nm}^{(ij)}(\text{bottom}) &= J_i(n, m, \eta, \nu, y_j) \\ C_{nm}^{(ij)}(\text{west}) &= K_i(m, n, \nu, \eta, x_j) \\ C_{nm}^{(ij)}(\text{east}) &= K_i(m, n, \nu, -\eta, x_j) \\ C_{nm}^{(ij)}(\text{top}) &= J_i(n, m, \eta, -\nu, y_j) \\ S_{nm}^{(ij)}(\text{bottom}) &= K_i(n, m, \eta, \nu, y_j) \\ S_{nm}^{(ij)}(\text{west}) &= J_i(m, n, \nu, \eta, x_j) \\ S_{nm}^{(ij)}(\text{east}) &= J_i(m, n, \nu, -\eta, x_j) \\ S_{nm}^{(ij)}(\text{top}) &= K_i(n, m, \eta, -\nu, y_j) \end{aligned}$$

and finally:

$$\begin{aligned} C_{nm}^{(ij)}(\text{north}) &= L(n, m, \eta, \nu, x_i, y_j) \\ S_{nm}^{(ij)}(\text{north}) &= L(m, n, \nu, \eta, y_j, x_i) \end{aligned}$$

The reduced double integrations are given in the next four sections.

### 13.1 Reduced Isotropic Functional $H_i(n, m, a, b, c)$

Let:

$$\begin{aligned} A_i(u) &= \sqrt{a^2(u+1)^2 + Z_i^2} \\ C_m^k &= \frac{m!}{k!(m-k)!} \\ \alpha &= \frac{c+b}{A_i} \\ \beta &= \frac{c-b}{A_i} \\ h(\xi) &= \xi^k(\xi+1)\arctan(\xi) - \frac{\xi^k}{k} \end{aligned}$$

where  $\xi$  is a real variable.

Then:

$$H_i(n, m, a, b, c) = \int_{-1}^{+1} \frac{u^n(u+1)}{2A_i} f_m^{(i)}(u) du \quad (13.5)$$

where:

$$f_m^{(i)}(u) = \frac{A_i}{b^{m+1}} \sum_{k=0}^m (-1)^k A_i^k(u) C_m^k c^{(m-k)} g_k^{(i)}(u) \quad (13.6)$$

with  $g_k^{(i)}(u)$  given by the following recurrence relation:

$$(k+1)g_k^{(i)}(u) + kg_{k-1}^{(i)}(u) = h(\alpha) - h(\beta) \quad (13.7)$$

$$g_0^{(i)}(u) = \alpha \arctan(\alpha) - \beta \arctan(\beta) - \frac{1}{2} \ln\left(\frac{\alpha^2+1}{\beta^2+1}\right) \quad (13.8)$$

### 13.2 Reduced Azimuthal Functional $J_i(n, m, a, b, c)$

Let:

$$A_i(u) = \sqrt{a^2(u+1)^2 + Z_i^2}$$

$$E = \sqrt{(c-b)^2 + A_i^2} - \sqrt{(c+b)^2 + A_i^2}$$

then:

$$J_i(n, m, a, b, c) = \int_{-1}^{+1} \frac{u^n(u+1)^2}{3A_i^2} f_m^{(i)}(u) du \quad (13.9)$$

where:

$$f_m^{(i)}(u) = c g_m^{(i)}(u) - b g_{m+1}^{(i)}(u) \quad (13.10)$$

$g_m^{(i)}(u)$  being given by the following recurrence relation:

$$mb^2 g_m^{(i)}(u) - (2m-1)bc g_{m-1}^{(i)}(u) + (m-1)(c^2 + A_i^2) g_{m-2}^{(i)}(u) = E \quad (13.11)$$

$$g_0^{(i)}(u) = \frac{1}{b} \ln \left( \frac{\sqrt{(b-c)^2 + A_i^2} + (b-c)}{\sqrt{(b+c)^2 + A_i^2} - (b+c)} \right) \quad (13.12)$$

$$g_1^{(i)}(u) = \frac{E}{b^2} + \frac{c}{b} g_0^{(i)}(u) \quad (13.13)$$

### 13.3 Reduced Azimuthal functional $K_i(n, m, a, b, c)$

Let:

$$A_i(u) = \sqrt{a^2(u+1)^2 + Z_i^2}$$

$$E = \sqrt{(c-b)^2 + A_i^2} - \sqrt{(c+b)^2 + A_i^2}$$

then:

$$K_i(n, m, a, b, c) = \int_{-1}^{+1} \frac{u^n(u+1)}{3} f_m^{(i)}(u) du \quad (13.14)$$

where:

$f_m^{(i)}(u)$  being given by the following recurrence relation:

$$mb^2 f_m^{(i)}(u) - (2m-1)bc f_{m-1}^{(i)}(u) + (m-1)(c^2 + A_i^2) f_{m-2}^{(i)}(u) = E \quad (13.15)$$

$$f_0^{(i)}(u) = \frac{1}{b} \ln \left( \frac{\sqrt{(b-c)^2 + A_i^2} + (b-c)}{\sqrt{(b+c)^2 + A_i^2} - (b+c)} \right) \quad (13.16)$$

$$f_1^{(i)}(u) = \frac{E}{b^2} + \frac{c}{b} f_0^{(i)}(u) \quad (13.17)$$

### 13.4 Reduced Azimuthal Functional $L(n, m, a, b, c, d)$

Let:

$$D(u) = \sqrt{(c-au)^2 + 4\mu^2}$$

$$E = \sqrt{(d-b)^2 + D^2} - \sqrt{(d+b)^2 + D^2}$$

then:

$$L(n, m, a, b, c, d) = \int_{-1}^{+1} \frac{u^n}{3D^2(u)} f_m(u) du \quad (13.18)$$

where:

$$f_m(u) = dg_m(u) - bg_{m+1}(u) \quad (13.19)$$

$g_m(u)$  being given by the following recurrence relation:

$$mb^2g_m(u) - (2m - 1)bdg_{m-1}(u) + (m - 1)(d^2 + D^2)g_{m-2}(u) = E \quad (13.20)$$

$$g_0(u) = \frac{1}{b} \ln \left( \frac{\sqrt{(b-d)^2 + D^2} + (b-d)}{\sqrt{(b+d)^2 + D^2} - (b+D)} \right) \quad (13.21)$$

$$g_1(u) = \frac{E}{b^2} + \frac{d}{b}g_0(u) \quad (13.22)$$

## 14. APPENDIX B. FORTRAN PROGRAM FOR NUMERICAL INTEGRATION

For microcomputer programs by Legendre-Gauss quadrature.

C        This subroutine QUAD1 computes a single integral numerically,  
C        the limits are from -1 to +1, the user must provide the  
C        function FX(X).  
C        RES contains the numerical estimate of the integral.

```

SUBROUTINE QUAD1(NMAX,RES)
REAL WT(10),XU(10)
CALL LEGR(XU,WT,NMAX)
RES=0.
DO 1 L=1,NMAX
X=XU(L)
RES=RES+FX(X)*WT(L)
1        CONTINUE
RETURN
END
C        -----
```

C This subroutine QUAD2 computes a double integral numerically,  
C the limits are from -1 to +1 in both integrals,the user must  
C provide the function FXY(X,Y).RES contains the numerical  
C estimate of the integral.

```
SUBROUTINE QUAD2(NMAX,RES)
```

```
REAL WT(10),XU(10)
```

```
CALL LEGR(XU,WT,NMAX)
```

```
RES=0.
```

```
DO 1 M=1,NMAX
```

```
X=XU(M)
```

```
WTM=WT(M)
```

```
DO 1 N=1,NMAX
```

```
Y=XU(N)
```

```
RES=RES+FX(X,Y)*WT(N)*WTM
```

```
1 CONTINUE
```

```
RETURN
```

```
END
```

```
C
```

```
-----  
C This subroutine QUAD3 computes a triple integral numerically,  
C The limits are from -1 to +1 in all 3 integrals,the user must  
C provide the function FXYZ(X,Y,Z). RES contains the numerical  
C estimate of the integral.
```

```
SUBROUTINE QUAD3(NMAX,RES)
REAL WT(10),XU(10)
CALL LEGR(XU,WT,NMAX)
RES=0.
DO 1 M=1,NMAX
X=XU(M)
WTM=WT(M)
DO 1 N=1,NMAX
Y=XU(N)
WTN=WT(N)
DO 1 L=1,NMAX
Z=XU(L)
RES=RES+FXYZ(X,Y,Z)*WTM*WTN*WT(L)
1 CONTINUE
RETURN
END
C -----
C This subroutine LEGR contains the weights to be used in the
C numerical integration process.

SUBROUTINE LEGR(XU,WT,NMAX)
REAL XU(10),WT(10)
```

```
IF(NMAX.GT.10.OR.NMAX.LT.0)THEN
PRINT*,'NMAX must be 1 to 10'
STOP
ENDIF
IF(NMAX.EQ.1)THEN
XU(1)=0.0
WT(1)=2.0
    ELSE IF(NMAX.EQ.2)THEN
XU(1)=-0.5773502692
WT(1)=1.
    ELSE IF(NMAX.EQ.3)THEN
XU(1)=-0.7745966692
XU(2)=0.0
WT(1)=0.555555555556
WT(2)=0.888888888889
    ELSE IF(NMAX.EQ.4)THEN
XU(1)=-0.8611363116
XU(2)=-0.3399810436
WT(1)=0.3478548451
WT(2)=0.6521451549
    ELSE IF(NMAX.EQ.5)THEN
XU(1)=-0.9061898459
XU(2)=-0.5384693101
```

```
XU(3)=0.  
WT(1)=0.2369268850  
WT(2)=0.4786286705  
WT(3)=0.5688888889  
ELSE IF(NMAX.EQ.6)THEN  
XU(1)=-0.9324695142  
XU(2)=-0.6612093865  
XU(3)=-0.2386191860  
WT(1)=0.1713244923  
WT(2)=0.3607615730  
WT(3)=0.4679139346  
ELSE IF(NMAX.EQ.7)THEN  
XU(1)=-0.9491079123  
XU(2)=-0.7415311856  
XU(3)=-0.4058451514  
XU(4)=0.  
WT(1)=0.1294849661  
WT(2)=0.2797053915  
WT(3)=0.3818300505  
WT(4)=0.4179591837  
ELSE IF(NMAX.EQ.8)THEN  
XU(1)=-0.9602898565  
XU(2)=-0.7966664774
```

```
XU(3)=-0.5255324099
XU(4)=-0.1834346425
WT(1)=0.1012285363
WT(2)=0.2223810345
WT(3)=0.3137066459
WT(4)=0.3626837834
ELSE IF(NMAX.EQ.9)THEN
XU(1)=-0.9681602395
XU(2)=-0.8360311073
XU(3)=-0.6133714327
XU(4)=-0.3242534234
XU(5)=0.
WT(1)=0.0812743884
WT(2)=0.1806481607
WT(3)=0.2606106964
WT(4)=0.3123470770
WT(5)=0.3302393550
ELSE IF(NMAX.EQ.10)THEN
XU(1)=-0.9739065285
XU(2)=-0.8650633666
XU(3)=-0.6794095683
XU(4)=-0.4333953941
XU(5)=-0.1488743390
```

WT(1)=0.0666713443

WT(2)=0.1494513491

WT(3)=0.2190863625

WT(4)=0.2692667193

WT(5)=0.2955242247

ENDIF

NMID=NMAX/2

DO 9 N=1,NMID

NP=NMAX+1-N

WT(NP)=WT(N)

XU(NP)=ABS(XU(N))

9 CONTINUE

RETURN

END

## 15. APPENDIX C. TEST FOR MODEL'S APPLICABILITY

The following is a computer program that tests the model's applicability in the nodal method (it can also be extended to any situation). It has been assumed that the user has already produced, by a program not included, the four transfer matrices associated with each of the four components of the angular flux. These should be named MATRANF.ISO, MATRANF.COS, MATRANF.SIN and MATRANF.RAD. The matrix transfer for the isotropic component is a 30 x 15 matrix, the three others are 30 x 10 matrices.

```

      INTEGER I,J,S
      REAL CURR,ETA,NU,MU,ISO,OFW,IFW,r
      DIMENSION A(450),B(300),ANG(10),COF(15)
      OPEN(UNIT=11,STATUS='OLD',FILE='MATRANF.ISO')
      OPEN(UNIT=13,STATUS='OLD',FILE='MATRANF.COS')
      OPEN(UNIT=15,STATUS='OLD',FILE='MATRANF.SIN')
      OPEN(UNIT=17,STATUS='OLD',FILE='MATRANF.RAD')
      ISO=0.0
C      Enter here the dimensions of the void
      ETA=
      NU=

```

```
MU=
C   IFW is the total number of neutrons entering through the
C   unique source face.
   IFW=4.18879*ETA*NU*(10.0+(4.0/MU))
   READ(11,*) (A(I),I=1,450)
   DO 23 J=2,15
   COF(J)=0.0
23  CONTINUE
   COF(1)=4.0
   COF(4)=-1.0/(ETA**2)
   COF(5)=-1.0/(NU**2)
   DO 24 I=1,30
   CURR=0.0
   DO 25 J=1,15
   CURR=CURR+A(30*(J-1)+I)*COF(J)
25  CONTINUE
   ISO=ISO+CURR
24  CONTINUE
   DO 19 S=2,4
31  IF(S.EQ.2) THEN
   READ(13,*) (B(I),I=1,300)
   GO TO 61
   ELSE
```

```
GO TO 41
ENDIF
41  IF(S.EQ.3) THEN
    READ(15,*) (B(I),I=1,300)
    GO TO 61
    ELSE
    GO TO 51
    ENDIF
51  IF(S.EQ.4) READ(17,*) (B(I),I=1,300)
61  DO 20 J=1,10
    ANG(J)=0.0
20  CONTINUE
    IF(S.EQ.2) ANG(2)=2.0/(ETA**2)
    IF(S.EQ.3) ANG(3)=2.0/(MU**2)
    IF(S.EQ.4) ANG(1)=2.0/MU
    DO 21 I=1,30
    CURR=0.0
    DO 22 J=1,10
    CURR=CURR+B(30*(J-1)+I)*ANG(J)
22  CONTINUE
    ISO=ISO+CURR
21  CONTINUE
19  CONTINUE
```

```
C      OFW is the total number of neutrons that exits from all faces.
      OFW=ISO
C      Compute the relative neutron balance and print result of test.
      r=ABS(IFW-OFW)/IFW
      IF(r.GE.0.0015) THEN
      PRINT*,'This model is not applicable!'
      ELSE
      PRINT*,'This model is applicable!'
      STOP
      END
```

